# AN ELECTRON GUN AND BEAM SPREADING

A Thesis submitted to McGill University in partial fulfilment of the requirements for the Degree of Master of Science by

Cyril J. Tunis. B.Eng.

April 1956.

## Acknowledgments.

Grateful acknowledgment is due to Dr. S. Wagner, my research supervisor; Professor G.A. Woonton, Director of the Eaton Electronics Laboratory at which this work was done; Ross McFarlane, M.Sc., Robert Vessot, M.Sc., Alec Szabo, M.Sc., fellow students who taught me much; Bob Lorimer, who did the glass work; and Mr. A.V. Averlaid, who transformed the gun and tube designs from idea to reality.

The equipment used was supplied to the Laboratory under a grant by the Defence Research Board. The author was the grateful holder of a National Research Council Bursary while performing this work.

TABLE OF CONTENTS

## LIST OF FIGURES.



## LIST OF GRAPHS

## LIST OF PLATES.

## Introduction.

In recent years the development of radio communication and of allied techniques such as radar and television has involved the use of higher and higher frequency signals. This trend has arisen, either from the need of more channels in the useful frequency spectrum, or, as in radar, from the need of directional antenna systems of reasonable size.

In tubes of conventional design the upper limit of the useful frequency range is set by considerations of transit time of electrons, radiation losses and inductance of leads. The design of conventional tubes has been improved to permit them to operate at frequencies up to hundreds of megacycles per second, but the microwave region (1,000 to 40,000 megacycles per second) has been truly exploited by new types of amplifiers such as the klystron, the magnetron, the carcinatron and the travelling wave tube. These are capable of producing frequencies as high as 40,000 megacycles per second in commercially available forms.

The resonant parts of these tubes, that is, those parts which determine the operating frequency, become necessarily smaller as the frequency increases. These tubes utilise electron beams as an integral part and at the higher frequencies the electron beam must occupy a smaller and smaller volume, and so current density must be increased. A high current density beam is difficult to achieve because as the electrons become crowded more closely the mutual forces of repulsion increase and tend to make the beam spread. It is only within the last ten years that tubes have been designed in which the space charge repulsion in the beam has been a serious problem, and despite great progress in this field there is still much to be desired in the quality of high density electron beams.

The electron stream required in devices such as cathode ray or television tubes is produced by an electron gun. A particular type of high current density gun is the "Pierce" type electron gun. This thesis is concerned, in part, with the design and operation of an improved and particularly convenient Pierce gun.

In actual use, in a high frequency device, the electron beam formed by the gun is confined against the forces of space charge spreading by a magnetic field. In order to properly confine an electron beam it is necessary to know how the beam would behave if allowed to spread. A recent work has predicted theoretically the beam spread due to space charge and thermal velocity effects. This present work attempts to obtain measurements of actual beam spreading and to compare the measured beam spreads with those predicted by the theory.

# 1. THEORY.

## 1.1. Pierce Guns.

An electron gun, ideally, represents a source of electrons, all moving with the same velocity and in the same direction i.e., a beam of electrons. There is a source of electrons in every commercial vacuum, or radio tube - but it would not be termed a "gun" unless it shaped the emitted electrons into a well defined beam. In many vacuum tubes the electrons are emitted from an incandescent wire or coated surface, called the cathode, and attracted, by virtue of an electric field, to a plate surrounding the cathode, called the anode electrode.

The simplest gun one could build would probably look like the one shown in Figure 1. Here is shown a coated disc, which emits the electrons, being indirectly heated by a coil of wire. This cathode would be centrally located behind an aperture in a disc-like electrode, to be called the cathode electrode. The cathode and cathode electrode would be at the same potential or voltage (zero, usually) in order that the electron paths would not be affected by fields between them. Parallel to the cathode electrode, and at a positive potential with respect to it, is a similarly apertured disc - the anode electrode. If the apertures involved are small enough so as not to disturb greatly the electric fields between the two electrodes, which exist by virtue of the potential difference between them - then electrons will start off at the cathode, (we assume with zero velocity), be attracted by the electric field towards the anode, and move through the anode aperture with a velocity corresponding to the anode potential. Thus, a beam of electrons would come out of the anode aperture, containing all the electrons emitted by the cathode, moving in straight lines perpendicular to the cathode surface.

This picture is exceedingly simple - for it ignores the effect of the apertures on the electric fields; the tendency of electrons to repel one another because of their similar negative charge, (space charge effect) and the random, but finite, velocities which the electrons possess as they are emitted from the cathode ("thermal velocities"). These considerations result in only a fraction of the emitted electrons passing through the anode aperture - the remainder impinge on the anode electrode itself and are lost as useful beam electrons.

The space charge effect depends on the number of electrons per unit volume of the beam and thus will be more severe the higher the beam current density. If the current required of an electron gun is not too large (say in the microampere range, as in most cathode ray tubes) then the loss of current to the anode is of no great consequence - the electrons impinging on the anode electrode will heat it and thus represent a small loss of power. However if, as in most high frequency tubes, it is desired to obtain a beam of reasonable current (milliampere range), combined with a relatively high current density, then the space charge effect is more severe. A greater fraction of the beam electrons are lost to the anode electrode, and, not only does this limit the available beam current, but the consequent power lost to the anode electrode becomes prohibitively serious. It may also be desired that the current density in the beam be greater than that at the surface of the cathode and this could be done by "converging" the beam of electrons as it leaves the cathode surface. Again, space charge would oppose any such converging action.

It becomes apparent that the designer of any gun intended to supply a high current density beam must inevitably take into consideration the mutual repulsion of the electrons in the beam.

In general, the mathematical determination of electron paths under conditions of "space charge" repulsion (ignoring thermal effects) is extremely difficult. The laws of space charge flow are known for only a limited number of simple cathode-anode geometries, such as plane, cylindrical and spherical. In these particular configurations the electrons flow in straight lines and their velocity, or potential, at any point is directly related to the distance from the cathode to that point. The most universally used high current-density electron gun is based on a design due to Pierce - and in Figure 2 is shown the principle on which a "converging" type of "Pierce" gun is based.

At (a) is shown two concentric spheres - the outer one may have an emitting coating on its inside surface and thus acts as a cathode, while the inner sphere could be made the anode. Space charge limited electron flow could then exist between them. A converging cylindrical beam is represented by only a segment of the concentric sphere cathode-anode system as at (b). Mathemat-

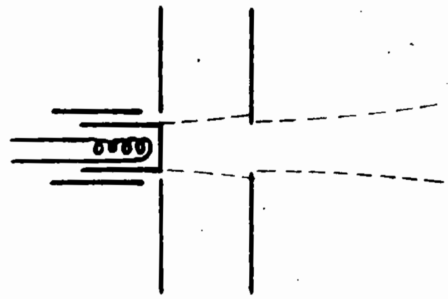

Figure 1: Crude Electron Gun

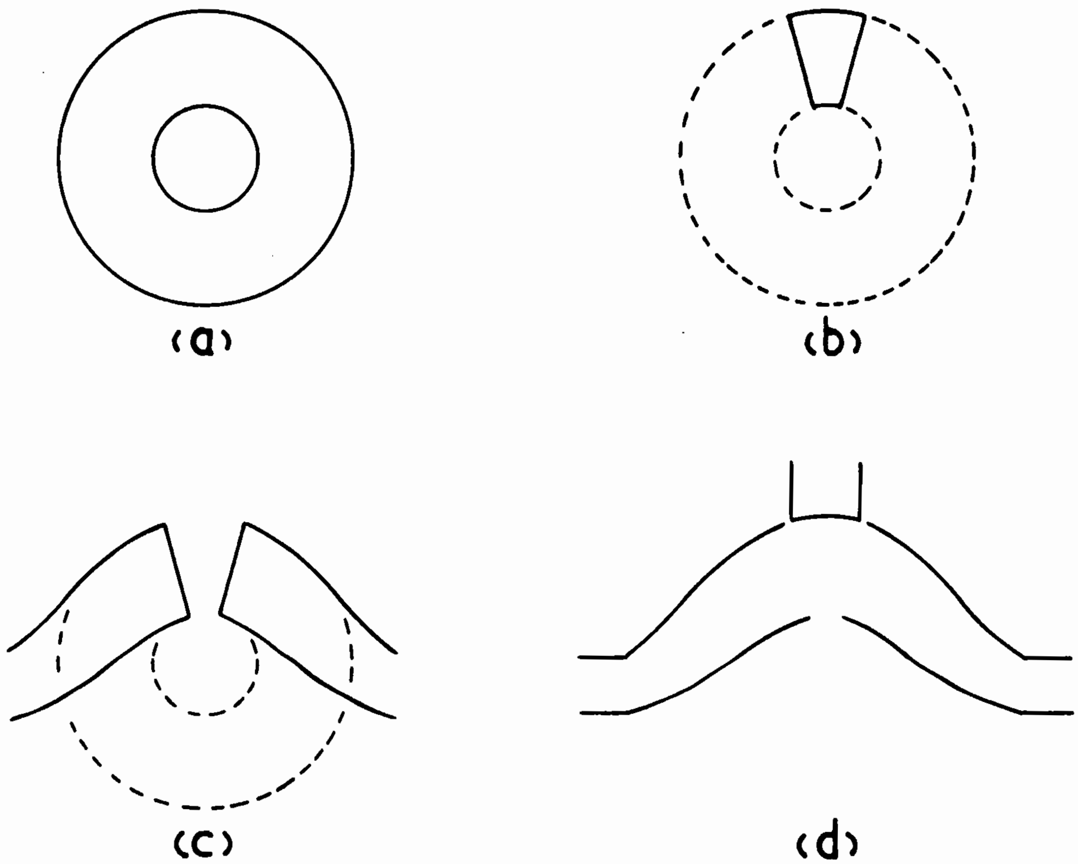


Figure 2: Development of Pierce Shapes

ically, the electron paths and velocities for space charge limited flow between the concentric spheres can be determined. The voltage variation with radius between the spheres is known. Pierce suggested that a segment of this flow could be obtained by replacing the remainder of the concentric sphere system by electrodes, so shaped that the voltage variation along the edges of the desired segment would be the same as when the concentric sphere system was complete. This is illustrated in (c) and a Pierce gun, using these electrode shapes so determined, is shown at (d). With an aperture in the anode electrode, this gun should produce a beam of electrons, all of which pass through the anode aperture and with a current density higher than that at the cathode surface.

The following paragraphs indicate the mathematical analysis which yields the design information for the "Pierce Gun".

The current in a circular conical section of the space charge limited radial flow between two concentric spheres (as shown in Figure 2) is given by

$$I = \frac{0.928 \sin^2 (\theta/2) \, (V_{kv})^{3/2}}{\alpha^2} \qquad (1)$$

where

$V_{kv}$ - beam voltage in kilovolts.

$\theta$ - semiangle of the cone

$\alpha$ - is a function of $r/r_c$

$r_c$ - radius of outer sphere

The voltage may then be written as a function of the radius

$$V_{kv} = \frac{1.051\ I^{2/3}}{(\sin {}^{\theta}/2)^{4/3}}\ \alpha^{4/3} \qquad (2)$$

since $\alpha$ is a function of $(^r/r_c)$. This is the voltage variation that must be produced by the electrode shapes in order to maintain the flow. There is, however, another "boundary condition" - and this is that the voltage at any radius must not change with the angle $\theta$ - this is stated:

$$\frac{dV}{d\theta} = 0 \qquad (3)$$

If the two conditions stated in (2) and (3) are fulfilled, and ignoring thermal velocity effects, a conical beam of semi-angle $\theta$ comes off the cathode and out through the anode aperture. However, the effect of the aperture on the electric field between the cathode and anode electrodes must be taken into account.

The anode aperture acts as an "aperture lens" [1] causing the beam to leave the anode less convergent than on entering it. Assuming the electric field is zero beyond the anode aperture, the focal length of the anode aperture lens is

$$f = 4V/E \qquad (4)$$

where

- V - is anode potential
- E - is electric field strength on cathode side of aperture.

Using equations (4) and (2) results in

$$\frac{f}{r_c} = \frac{-3\alpha}{d\alpha/dR} \tag{5}$$

where

R is equal to $^{r}/r_c$.

Since $\alpha$ is a function of $^{r}/r_c$, then $^{f}/r_c$ can be expressed as a function of $^{r}/r_c$. At the anode aperture, r is of course, the radius of the anode sphere $r_a$. Thus the focal length of the anode aperture is dependent only on $^{r_a}/_{r_c}$.

The gun geometry is shown in Figure 3. Using the nomenclature shown, the lens formula (from optics) may be written

$$\frac{1}{r_a} - \frac{1}{b} = \frac{1}{f} \tag{6}$$

and the exit angle, $\gamma$, of the beam can be deduced from geometry as

$$\frac{\sin\theta}{\sin\gamma} = \frac{b}{r_c}\ \frac{r_c}{r_a} \tag{7}$$

By rewriting equation (6) thusly

$$\frac{b}{r_c} = \frac{1}{^{r_c}/_{r_a} - {}^{r_c}/_{f}} \tag{8}$$

it can be seen that both b and $\gamma$ are dependent only on the ratio of cathode to anode radius $^{r_c}/_{r_a}$. It should be mentioned here of course, that in considering the lens action of the anode aperture on the beam we have ignored space charge effects.

There is now sufficient information to design a Pierce Gun - neglecting, at this time, the problem of determining the correct

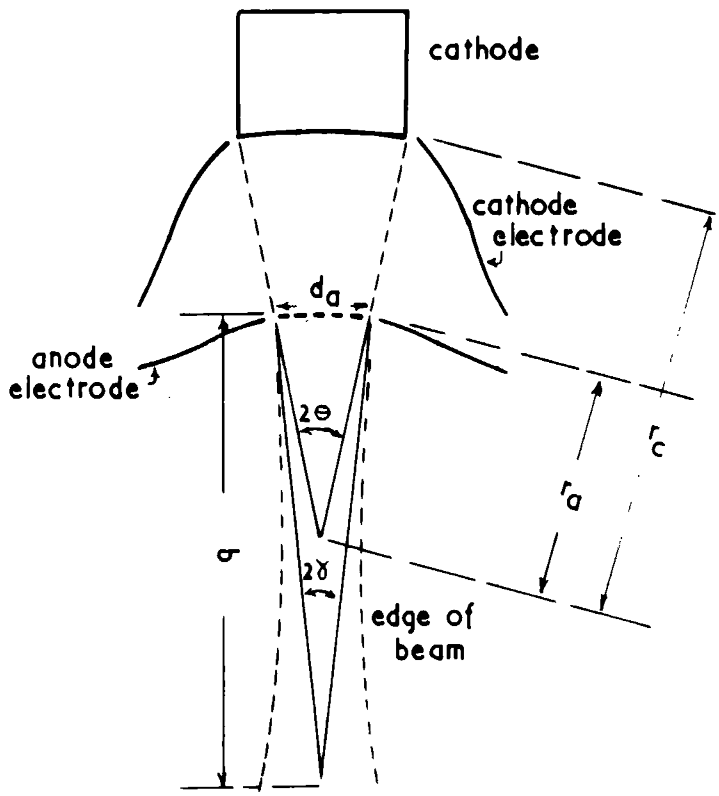


Figure 3: Gun Geometry
(after Spangenberg)

electrode shapes.

Equation (1) reveals that any two of the four quantities I, V, $\theta/2$, $r_c/r_a$ ($\alpha$), may be chosen to conform to specific requirements. The quantity $I/(V_{kv})^{3/2}$ is constant for any gun and is a useful beam parameter - it is defined as G, the beam perveance. Using (1),

$$G = \frac{0.928 \sin^2 \theta/2}{\alpha^2} \tag{9}$$

If a beam of specific perveance is required, then either $\theta/2$ or $\alpha^2$ may still be chosen by the designer, the other is determined by equation (9). Having done this, the focal length of the anode aperture is determined by (5), b may be found from (6) and the exit angle $\gamma$ from (7). The exit angle enables one to determine the beam shape after it emerges from the gun (see Part 2.2).

Nomographic charts of equations (5), (6) and (7) may be set up[1] and it is then a relatively simple matter to select values of $r_c/r_a$, $\theta$, and $\gamma$ for any desired voltage and current.

One must only make certain that the anode aperture is not so large as to disturb the fields in the cathode anode region. In general anode apertures should not be larger than one-half the cathode anode spacing. This statement applies, however, only if the electrode shapes are obtained from such a source as Reference (1), and not actually designed by the designer using an Electrolytic Tank, as described below.

## 1.2. The Electrolytic Tank.

The cathode and anode electrode shapes in a Pierce gun which provide the exact boundary conditions as given in equations (2) and (3) are spherically symmetrical but curved, as the shapes shown in Figure 2. An exact analytical method for the determination of these shapes has not yet been found, but one method of solving for the shapes utilizes the electrolytic tank.

Essentially the problem is one of electrostatics: an electric field must be set up, by virtue of the electrode shapes and the potential between them, which matches conditions (2) and (3) along a line representing the beam edge. These fields are outside the beam and on its edge - space charge need not be considered.

It is possible to solve electrostatic problems in an electrolytic tank [2] because the laws which govern the flow of current in a uniformly conducting medium are the same as the flows governing the distribution of electrostatic flux lines in a vacuum. Thus there exists a "one to one" correspondence between current density vector (J), specific conductivity (g) and potential (V) in the electrolyte and electric displacement vector (D), dielectric constant ($\epsilon$) and potential (V) in an electrostatic field. Lines of force in the electrostatic case become lines of current flow in the electrolyte. The relevant equations are:

$$\begin{aligned} J &= gE & \qquad D &= \epsilon E \\ \nabla \cdot J &= 0 & \qquad \nabla \cdot D &= 0 \\ \nabla^2 V &= 0 & \qquad \nabla^2 V &= 0 \end{aligned} \tag{10}$$

The analogy further requires that the conductance of the electrolyte be isotropic. This requirement may be violated at the boundaries of the fluid where polarisation may occur, but can be avoided by using alternating current in the range of 50 - 500 cycles per second. Any higher frequencies may introduce a reactive component due to the liquid-to-metal surfaces.

To obtain plots of electric field or potential distributions in any given electrostatic problem, electrodes are made to scale of copper (say) geometrically similar to the ones under consideration. The copper electrodes are immersed in the electrolyte, the proper potentials applied and the potential is plotted by probing the electrolyte with a vacuum tube voltmeter probe. It is not always necessary to represent the entire electrostatic electrode system in the tank; symmetrical cases allow considerable simplification. For instance, electrode configurations having cylindrical symmetry would have lines of force only in the radial and axial directions. Thus, the current flow model would have currents only in these two directions. It is possible to put insulating planes in the electrolyte perpendicular to the direction in which there is no current flow, hence enabling the representation of only a segment of the electrostatic system in the electrolytic tank. Figure 4 shows this principle in use - illustrating current flow models of concentric cylinders in plane and cylindrical symmetry and concentric spheres in cylindrical symmetry.

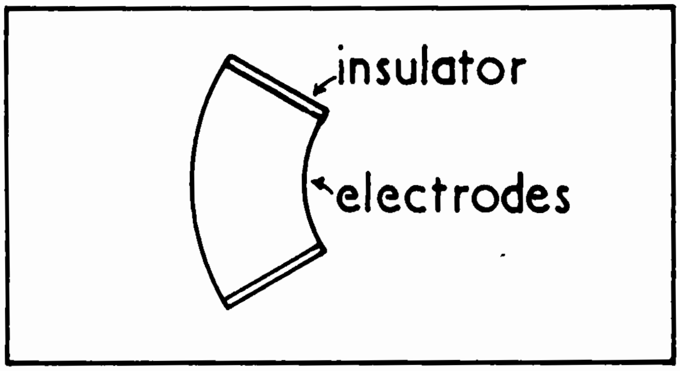


Concentric Cylinders in plane symmetry

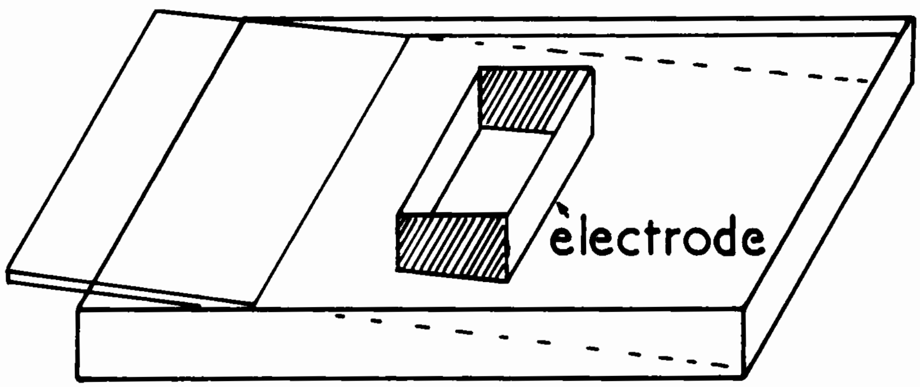


Concentric Cylinders in cylindrical symmetry

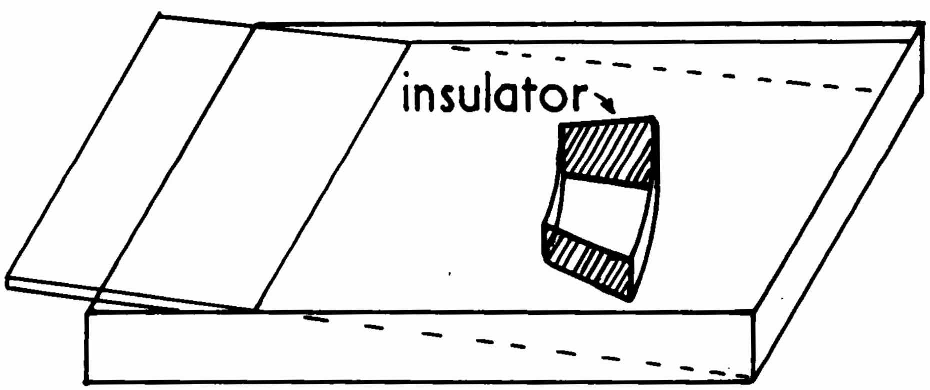


Concentric Spheres in cylindrical symmetry

Figure 4: Electrolytic Tank

In a similar manner we can determine the electrode shapes for, say, a Pierce gun, by immersing copper electrodes, in approximately the proper shape, in the electrolyte and deforming them until the proper field distribution is obtained. The resultant configuration may then be photographed or drawn and then the desired system, reduced to scale, is manufactured of suitable material.

## 1.3. Space Charge Spreading.

Up to this point, the action of the Pierce gun in effectively "focussing" the electrons as they come off the cathode into a converging "space charge flow" beam has been discussed. The effect of the anode aperture has been idealised to that of a thin lens and the defocussing effect of that lens calculated. The beam thus as it comes out of the gun will still be converging. The region beyond the gun, in most applications, is "field" free - there are no external electric forces on the beam - and it is called a "drift space". Here space charge spreading will manifest itself.

We have, of course, ignored thermal velocity effects assuming that the electrons originate from the cathode with zero initial velocity. This assumption implies that in the beam in the drift region:

(a) the flow of electrons is laminar, with no crossing of electron paths; and

(b) the electrons are uniformly distributed throughout the cross-section of the beam.

It may also, for purposes of further investigation, be reasonably assumed that in this drift space any longitudinal electric fields are uniform over a given cross-section of the beam.

Considering (a) and Gauss's Theorem it may be seen that the radial fields in the beam are proportional to the radius. If $\rho_v$ is the volumetric charge density, "r" the radius of the beam and E the radial electric field, then

$$\int E_r \cdot d\ell = \frac{1}{\epsilon_o} \int \rho_v \, dv \tag{11}$$

$$2 \pi r E = \rho_v / \epsilon_o \; \pi r^2 \tag{12}$$

$$E_r = \frac{\rho_v}{2 \epsilon_o} \cdot r \tag{13}$$

In order for the beam to maintain its uniform distribution of electrons, it must constrict uniformly. It is thus evident that the assumptions imply also that the radial velocity of any electron is proportional to the radius from the beam axis.

As the beam emerges converging from the gun, the space charge density $\rho_v$ will increase; $E_r$, or the outward force on the electrons will increase, and the inward radial velocity will be decreased till zero, when the electrons will all be flowing parallel. The radius of the beam will here be a minimum. From this point the radial velocity will become outward and the beam will spread, looking as in Figure 5. The beam may be analysed from the position of minimum radius $r_o$ and its subsequent spread

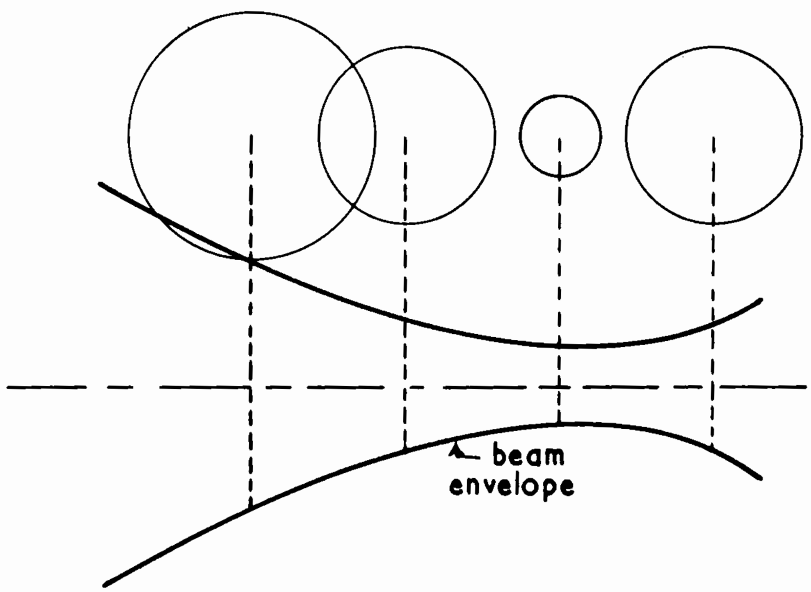


Figure 5: Space Charge Spreading
(after Spangenberg)

determined. For the outer electron, mass "m", charge "e", the force F is

$$F = eE = m\,\frac{d^2r}{dt^2} \tag{14}$$

Using (13)

$$m\,\frac{d^2r}{dt^2} = \frac{e\rho_{ov}}{2\epsilon_o}\,r_o \tag{15}$$

It is convenient to introduce the current and voltage, the measurable quantities, into the calculation. The current I is related to the volumetric charge density by

$$I = \pi r_o^2 \rho_o v \tag{16}$$

where "v" is the beam electron velocity which is related to V, the beam voltage by

$$V = \frac{1}{2}\,\frac{m}{e}\,v^2 \tag{17}$$

The problem is solved in Spangenberg's "Vacuum Tubes" in terms of "z", the axial distance from the beam minimum, and the result is

$$\frac{z}{r_o} = \frac{64.6}{\sqrt{G}} \int_0^{\sqrt{\ln R}} e^{t^2}\,dt \tag{18}$$

where

G is beam perveance $(I/V_{kv}{}^{3/2})$

R is $r/r_o$

The values of the integral in (18) may be found in Janke and Emdes "Tables of Functions", page 32.

This yields the Universal Space Charge Spreading Curve shown in Figure 6. The shape of the beam envelope, it will be noted, is the same for beams of the same perveance. The curve is also symettrical about z = 0.

From the Pierce gun data, the angle is known. The point on the Universal curve at which the slope is determines, with a knowledge of the beam perveance and beam radius at the anode, the position and size of the minimum beam radius as well as the subsequent beam shape in the drift space.

## 1.4. Thermal Velocities.

In all considerations of the electron flow, both in the gun region where the beam is shaped and in the drift region where the beam spreads due to space charge, the effects of thermal velocities have been ignored. They will be considered here according to the theory advanced by Cutler and Hines [(3)] a summary of which is presented below.

Electrons emitted off the surface of a hot cathode do not necessarily have zero velocities, as assumed heretofore, but may have finite velocities in all possible directions. The components of thermal velocities in the longitudinal direction of the beam do not significantly affect the beam shape for they are but a negligible fraction of the longitudinal velocities of the electrons, acquired as they are accelerated in the gun region. The transverse components of thermal velocities are of prime interest and a Maxwellian distribution of these velocities is assumed; the components are specified by:

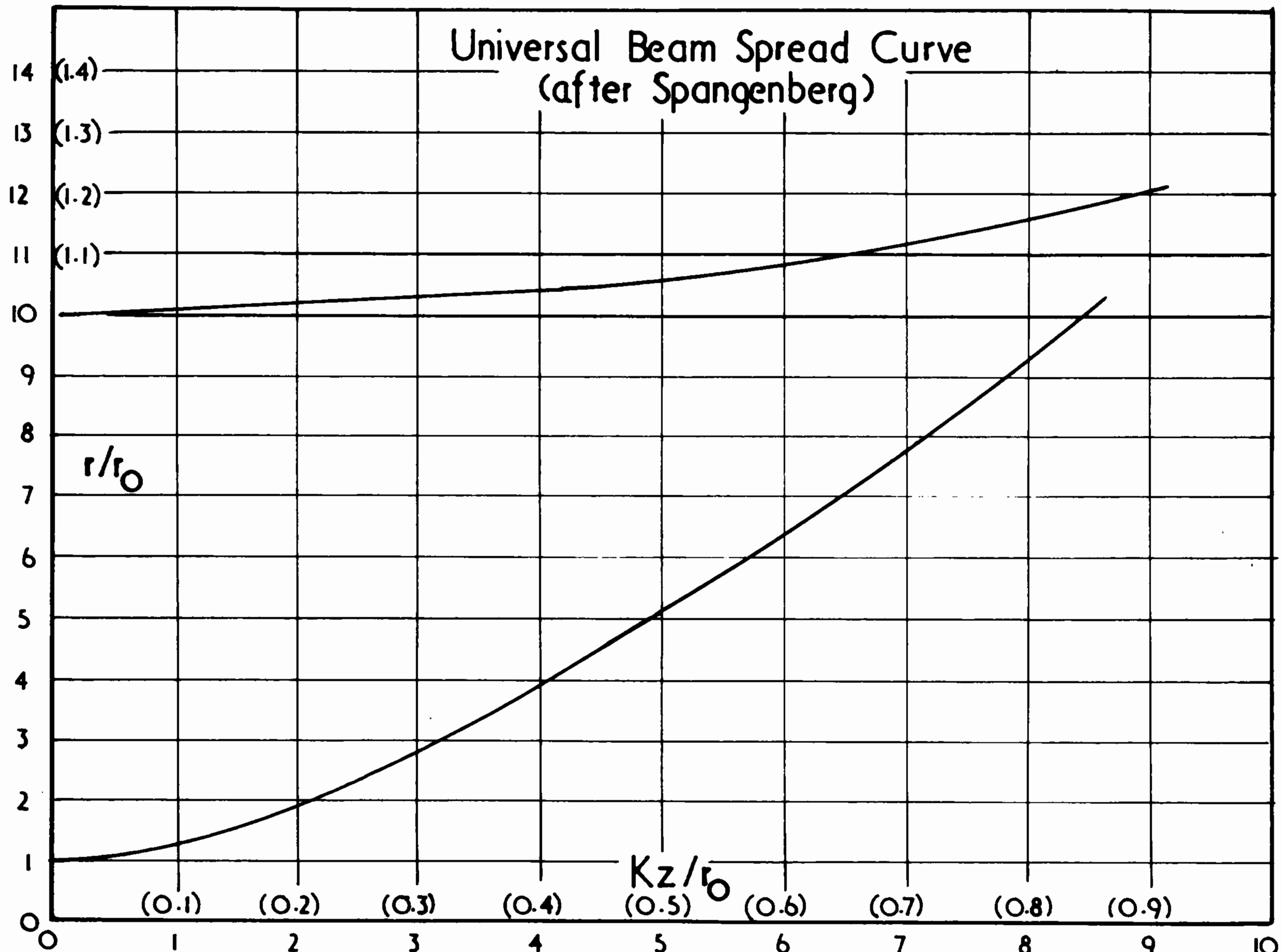
Universal Beam Spread Curve
(after Spangenberg)
$r/r_0$
$Kz/r_0$
14 (1.4)
13 (1.3)
12 (1.2)
11 (1.1)
10
9
8
7
6
5
4
3
2
1
0
0
1
2
3
4
5
6
7
8
9
10
(0.1)
(0.2)
(0.3)
(0.4)
(0.5)
(0.6)
(0.7)
(0.8)
(0.9)

Figure 6

$$d\,J_c = J_c \frac{m}{2\pi kT} e^{-(mv_x^2/2kT) - (mv_y^2/2kT)} dv_x\, dv_y \qquad (19)$$

where

$J_c$ is current density in "z" - direction at cathode surface

k - Boltzman's Constant

T - cathode temperature ($^{o}A$)

Using the distribution of transverse velocities, it is possible to determine the corrected electron trajectories both within the Pierce gun and in the drift space.

A radial co-ordinate "$\mu$" is defined which varies from zero on the beam axis to unity at the beam edge. Electrons emitted from the cathode with zero velocity would follow lines of constant $\mu$. If $r_e$ is the variable radius of the edge of the beam ($\mu = 1$) and r is the actual radial position of an electron moving in the beam

$$r = \mu\, r_e \qquad (20)$$

Differentiating twice,

$$\frac{d^2r}{dt^2} = r_e \frac{d^2\mu}{dt^2} + 2\frac{d\mu}{dt} + \mu \frac{d^2r_e}{dt^2} \qquad (21)$$

We assume, however, that laminar flow exists in the rest of the beam, except for the one electron under consideration. Hence, as before, the radial fields are proportional to distance from axis and we must have

$$\frac{d^2r}{dt^2} = \mu \frac{d^2r_e}{dt^2} \qquad (22)$$

rearranging (21) and (22)

$$\frac{d\,(d\mu/dt)}{d\mu/dt} = -2\,\frac{d\,r_e}{r_e}$$

integrating once gives

$$\ln \frac{d\mu}{dt} = -\ln r_e^{\,2} + \ln r_e^{\,2} + \ln\left(\frac{d\mu}{dt}\right)_1$$

where the subscript 1 indicates the value of the parameters at a fixed plane of reference. Taking antilogarithms

$$\frac{d\mu}{dt} = \left(\frac{d\mu}{dt}\right)_1 \frac{r_{e1}^{\,2}}{r_e^{\,2}} \tag{23}$$

integrating once again,

$$\mu - \mu_1 = \left(\frac{d\mu}{dt}\right)_1 \frac{dt}{(r_e/r_e\ )^2} \tag{24}$$

This is the fundamental equation for thermal trajectory tracing. The integral on the right-hand side involves only terms that are known for ideal laminar trajectories (space charge curve). Implicit in the work, however, is the assumption that the space charge trajectories are approximate to the actual trajectories. The integral limits are chosen to travel along the beam from the cathode through the Pierce gun and out to any point in the drift region.

ACCELERATING REGION - PIERCE GUN:- Equation (24) is utilised, the limits of integration being the "time" at the cathode and anode aperture - $t_c$ and $t_a$. From equation (2) may be written

$$V = K\alpha^{4/3} \qquad V_a = K\alpha_a^{\,4/3}$$

thus

$$V = \frac{V_a \, (\alpha)^{4/3}}{(-\alpha_a)^{4/3}} \tag{25}$$

where V is the voltage at a point between the cathode and anode, K is a constant, and the subscript "a" denotes the value of parameters at the anode aperture.

In an increment of time "dt" an electron will move a distance "$d\bar{r}$" at a velocity $\sqrt{2nV}$, hence

$$dt = \frac{-\,d\bar{r}}{\sqrt{2nV}} = -\,\frac{\bar{r}_e(-\alpha_a)^{2/3} \; d(\bar{r}/\bar{r}_c)}{\sqrt{2nV_a} \;\; (-\alpha)^{2/3}}$$

where equation (25) has been used and $\bar{r}_c$ is the radius of curvature at the cathode and $\bar{r}$ is the variable distance from points in the beam to the same centre. Substituting into the integral of (24), referring to the cathode ($r_{el} = r_c$) and using

$$\frac{\bar{r}}{\bar{r}_c} = \frac{r_e}{r_c}$$

which is true by virtue of radial flow, there results

$$\int_{t_c}^{t_a} \frac{dt}{(r_e/r_c)^2} = \frac{\bar{r}_c(-\alpha_a)^{2/3}}{\sqrt{2nV_a}} \int_{1}^{\bar{r}_c/\bar{r}_a} \frac{d(\bar{r}_c/\bar{r})}{(-\alpha)^{2/3}} \tag{26}$$

The integral on the right-hand-side (henceforth to be referred to as "A") may be plotted as a function of the upper limit and is shown in Figure 7. Thus from (24) and (26) the actual trajectory for an electron with a given initial transverse velocity may be determined in the gun region.

DRIFT REGION:- Beyond the anode aperture the beam diameter varies under the influence of the space charge forces within the beam, as discussed in section 1.3. Using (13),(14), (16), (17), the following is obtained.

$$\frac{d^2 r_e}{dt^2} = \frac{n\, I}{2\pi\epsilon \sqrt{2nV_a}\; r_e} \tag{27}$$

Using equation (1) for I and assuming $\theta$ is small enough so that sin $\theta$ may be approximated by $\theta$, equation (27) may be written

$$\frac{d^2 r_e}{dt^2} = \frac{2n\; V_a\; r_c^{\;2}}{9\;(-\alpha_a)^2\; \bar{r}_c^{\;2}} \cdot \frac{1}{r_e} \tag{28}$$

This may be put in integrable form by substituting

$$\omega = \frac{dr_e}{dt} \;; \qquad \omega \frac{d\omega}{dr_e} = \frac{d^2 r_e}{dt^2}$$

and upon integration

$$\frac{dr_e}{dt} = \pm \frac{\sqrt{2}\,\sqrt{2nV_a}}{3\;(-\alpha_a)} \quad \frac{r_e}{\bar{r}_c} \left[\ln \frac{r_e}{r_m}\right]^{1/2} \tag{29}$$

This includes the boundary condition that $dr_e/dt$ is zero at the minimum beam radius $r_m$. The positive sign is used for a diverging beam and the negative sign for a converging beam. Equation (29) and the substitution

$$\frac{r_e}{r_m} = e^{u^2}$$

may be used to write the integral of (24) for the drift region as

$$\int_{t_a}^{t} \frac{dt}{(r_e/r_c)^2} = 3\,\frac{\bar{r}_c\, r_e}{r_m} \sqrt{\frac{\pi/2\,(-\alpha_a)^2}{2\eta V_a}} \left[\frac{2}{\sqrt{\pi}} \int_0^{\sqrt{\ln r_a/r_m}} e^{-u^2}\, du \pm \frac{2}{\sqrt{\pi}} \int_0^{\sqrt{\ln r_e/r_m}} e^{-u^2}\, du\right] \tag{30}$$

The positive sign applies to points beyond the beam minimum. The two integrals on the right-hand side are error functions ( to be called "B" and "C" respectively) and may be plotted conveniently as shown in Figure 8.

The complete integral in (24) may now be used out to any point in the beam. The values of $r_e$, as a function of distance, are, of course, known from the original gun design and the space charge curve.

COMPLETE TRAJECTORY: GUN AND DRIFT TUBE REGIONS:- From (20) and (24), it can be seen that an electron will deviate from its nominal position by a distance $\Delta r$ given by

$$\Delta r = \left(\frac{dr}{dt}\right)_c \frac{r_e}{r_c} \int_{t_c}^{t} \frac{dt}{(r_e/r_c)^2} \qquad (31)$$

The two components of the integral are given in equations (30) and (26).

Thus a given electron starting off with a transverse velocity at the cathode of $(dr/dt)_c$ will arrive at some point down the beam a distance $\Delta r$ from its nominal line of laminar flow. This distance is given by equation (31). The equation as it stands is complete for a single electron - it must now be extended to the case of many electrons under the influence of thermal velocities.

The theory given above has been applied to one electron with an initial transverse velocity in the radial direction. Because of the linear character of the radial fields with radius, the initial derivation could have replaced "r" by either of its

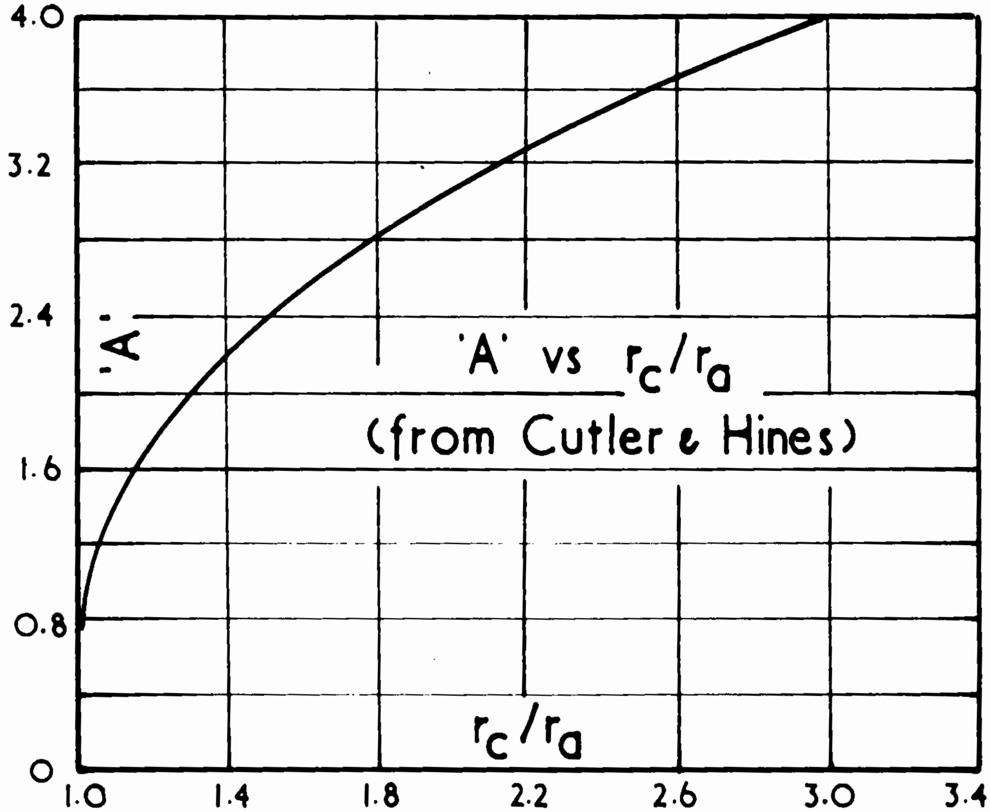


Figure 7

Figure 8

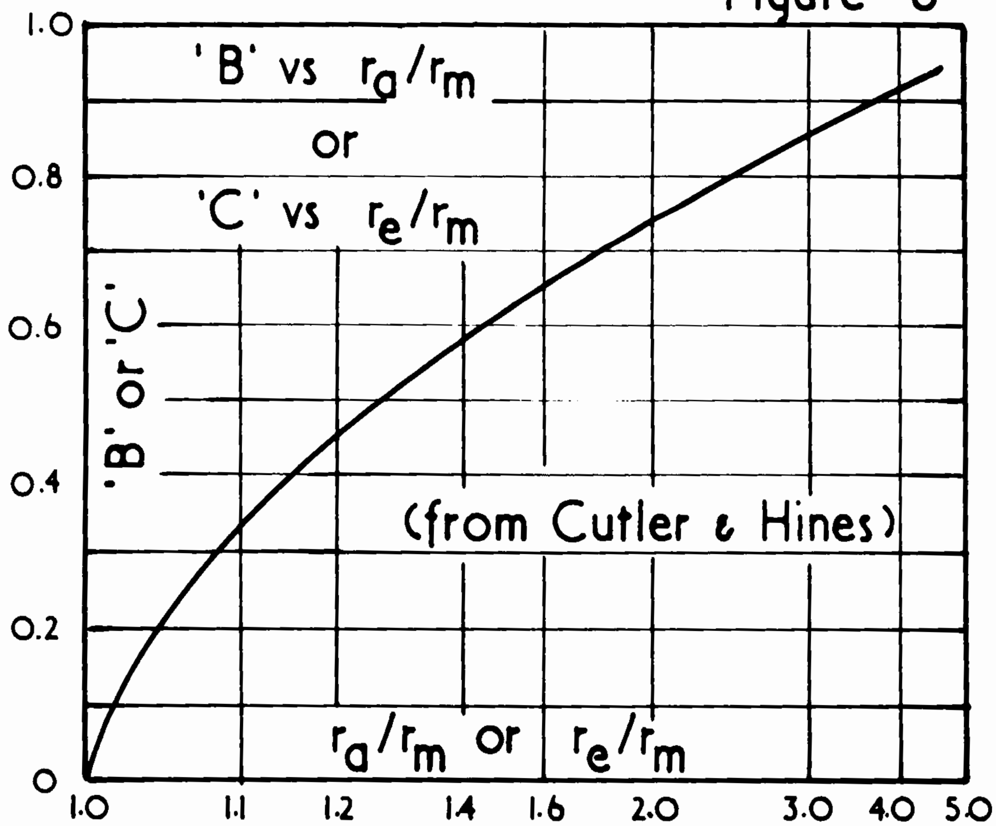

Cartesian co-ordinates, x or y and u by either $u_x$ or $u_y$. This could be carried right through to equation (31) - it may thus be seen that the magnitude of the deflection is independent of the direction of the initial velocity - a rather reasonable result in an axially symmetric system. To obtain the effect on the overall beam it is assumed that each electron moves in the field of the ideal beam and then this effect is summed over all electrons. If the beam is considerably spread then considerable error may result. Nevertheless, the theory does provide a first-order calculation of beam spreading and should be reasonably accurate unless the effect is quite large. It should be mentioned that, since most concern is with those electrons outside the nominal beam boundary, the inaccuracies of this theory tend to predict greater deviations than should actually occur in practice.

In Figure 9 is illustrated the geometry of the beam. The beam is considered at some cross-section along its length; current expected to arrive at a point Q will, in fact, be distributed symmetrically about Q, some of it arriving at a point P, distance "r" from the nominal beam center. The nominal beam radius at this cross-section is designated as $r_e$. The origin of the Cartesian co-ordinates x, y is put at the point Q.

It is convenient here to define a "normal deviation" where

$$\sigma = \frac{\Delta r}{\left(\frac{dr}{dt}\right)_c} \sqrt{\frac{kT}{m}} \tag{32}$$

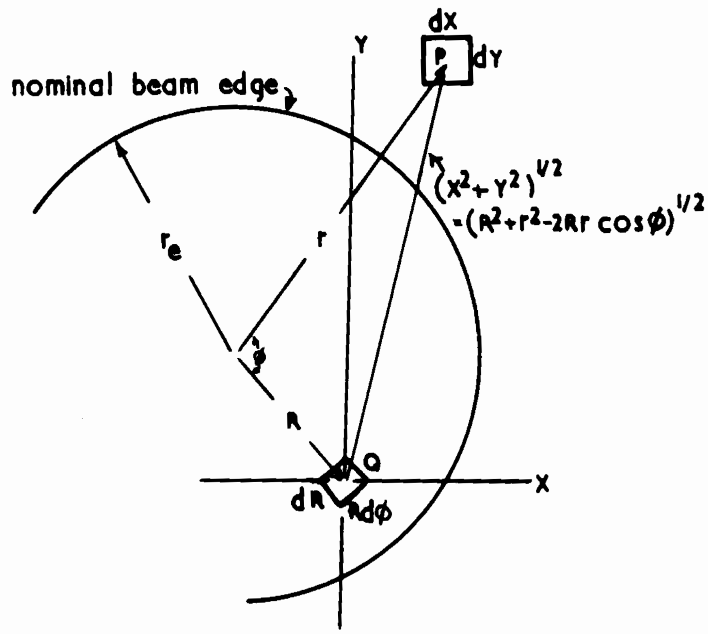


Figure 9: Beam Geometry
(after Cutler & Hines)

It follows from the above discussion that

$$\sigma = \frac{r}{(dr/dt)_c}\sqrt{\frac{kT}{m}} = \frac{x}{V_x}\sqrt{\frac{kT}{m}} = \frac{y}{V_y}\sqrt{\frac{kT}{m}} \tag{33}$$

where x and y are as shown in Figure 9.

It may be deduced from Figure 9 that the part of the current $dI_p$ which arrives at P, which would have arrived in the area at Q, is given by substituting x, y and $\sigma$ from (32) into (19) yielding

$$dI_p = \frac{J_o R dR d\phi}{2\pi} e^{-(x^2+y^2)/2r^2} \, d\left(\frac{x}{\sigma}\right) \, d\left(\frac{y}{\sigma}\right) \tag{34}$$

where $J_o$ is the beam current density in the absence of thermal effects. The current density at P from the area at Q is

$$dJ_p = \frac{dI_p}{dx\,dy} = \frac{J_o}{2\pi\sigma^2} \quad e^{-(x^2+y^2)/2\sigma^2} \quad RdRd\phi \tag{35}$$

Eliminating x and y by the law of cosines and integrating over the area of the nominal beam circle, then simplifying

$$\frac{Jr}{J_o} = e^{-r^2/2\sigma^2} \int_0^{r_e/r} \frac{R}{\sigma} \quad e^{-R^2/2\sigma^2} \quad I_o\left(\frac{Rr}{\sigma^2}\right) \, d\left(\frac{R}{\sigma}\right) \tag{36}$$

This last relationship yields the current density at any radius "r" in terms of the idealised beam current density, beam radius, and a parameter $\sigma$ which can be obtained from the gun design parameters. Using (33), (30) and (26), $\sigma$ may be written

$$\frac{r_e}{\sigma} = \frac{1}{\sqrt{\frac{kT}{2eV_a}}} \cdot \frac{\sin\theta}{(-\alpha_a)^{2/3} A + \frac{3r_c}{rm}\sqrt{\frac{\pi}{2}(-\alpha_a)^2}\,(B \pm C)}$$

where A, B, C have previously been defined and are plotted in

Figures 7 and 8.

Equation (36) can be evaluated by numerical integration and it gives a family of functions of normalised radius $r/r_e$ for various values of $r_e/\sigma$ . This is plotted in Figure 10. It may also be shown, as in Figure 11, the relation between the normalised radius as a function of $r_e/\sigma$ for various percentages of the total beam current enclosed. How this information was applied to experimental data will be described presently.

Using the theory allows the prediction of both the current density and beam radius variation with distance in a beam spreading due to both space charge and thermal velocities. A significant characteristic of this theory is that it predicts the beam minimum at points closer to the anode than under conditions of space charge spreading alone.

Figure 10

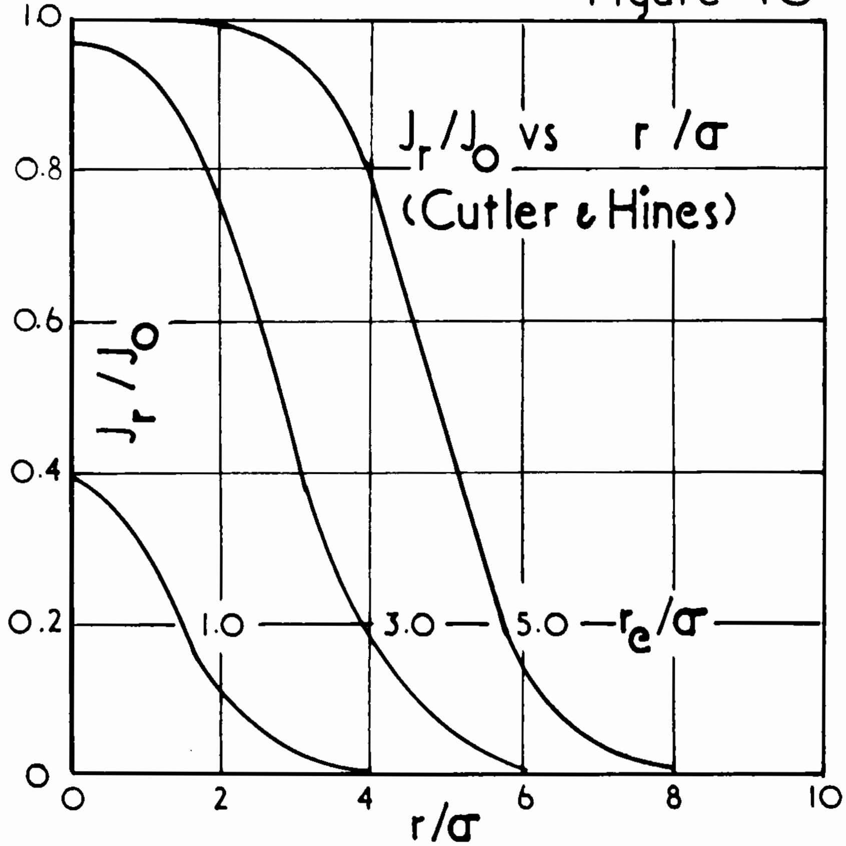


Figure 11

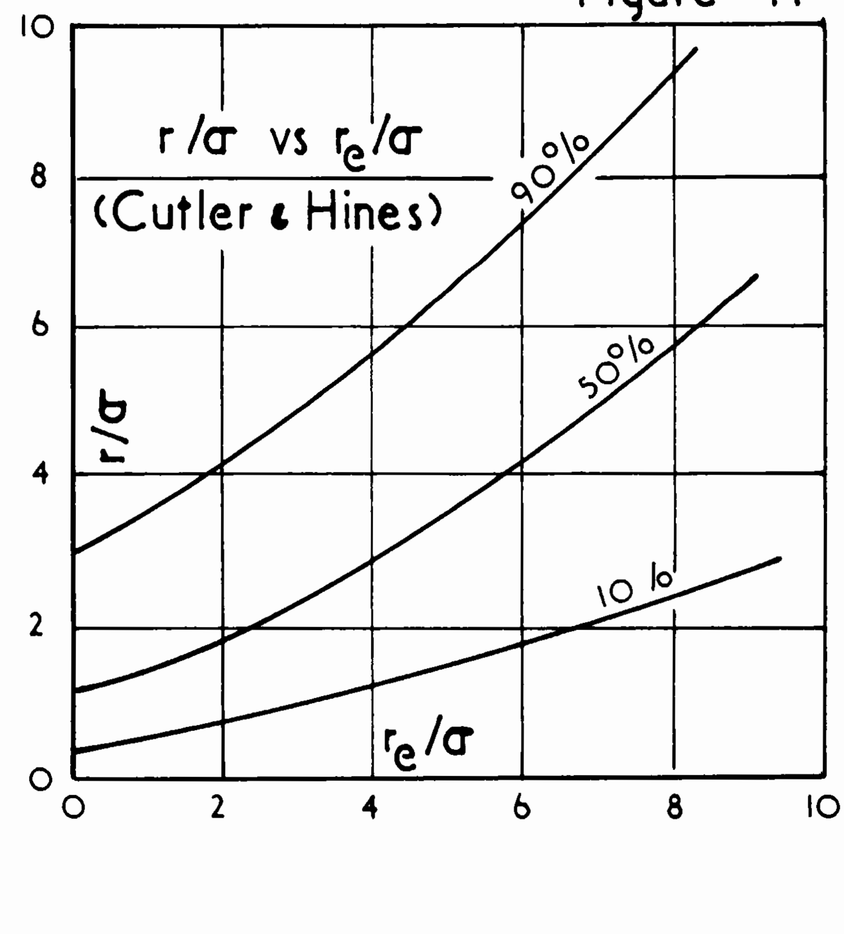

Figure 10(a)

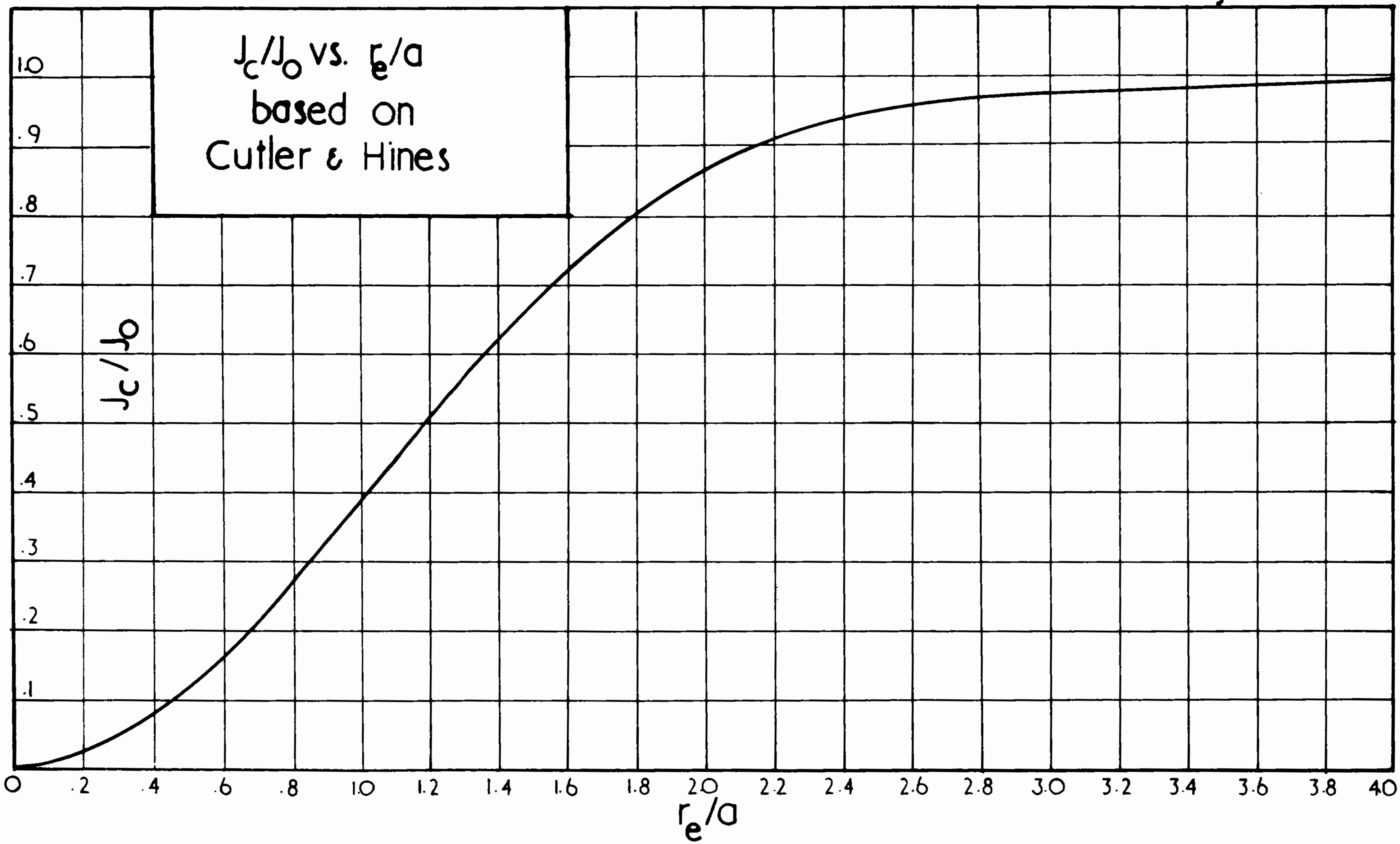

$J_c/J_o$ vs. $r_e/a$
based on
Cutler & Hines
1.0
.9
.8
.7
.6
.5
.4
.3
.2
.1
$J_c/J_o$
0
.2
.4
.6
.8
1.0
1.2
1.4
1.6
1.8
2.0
2.2
2.4
2.6
2.8
3.0
3.2
3.4
3.6
3.8
4.0
$r_e/a$

## 2. EQUIPMENT.

### 2.1. Electrolytic Tank.

It was desired to determine a set of electrode shapes for a Pierce type gun which could be built and handled more simply than conventional Pierce shapes. In addition other advantages were desired and are described in section 3.1. The shapes were determined by the use of an electrolytic tank; a physical description of which follows.

The tank was a rubber lined, rectangular container 24" x 36" and 5" deep. A glass plate with a ruled grid on it was also provided. The grid represented a reference for the positioning of the insulator and electrodes. The shapes desired possessed cylindrical symmetry so a wedge of water of angle 5 - 10$^{\circ}$ was used. This was obtained by tilting the glass plate with respect to the bottom of the tank, as shown in Figure 4.

The "water line" of the electrolyte in the tank represents the axis of symmetry of the electrode system. The tank was provided with levelling screws to enable the alignment of the water line along one of the ruled grid lines on the glass plate. The Electrolytic Tank is shown in Plate 1.

Referring to the theory of the Pierce gun the boundary condition (3) states that there must be no potential gradient across the beam edge. This implies that, in the electrolytic tank, there is to be no current flow across the beam edge. Hence the beam edge is represented by an ebonite insulator which, for a gun of semiangle $\theta$, is placed at an angle $\theta$ with respect to the water line, or axis of symmetry.

The electrodes must be shaped so as to provide a certain potential variation along the beam edge. The equation, in this case $V = K\alpha^{4/3}$ is solved to obtain the distance from the cathode along the beam boundary separated by equal increments (one-sixth of the total) of voltage. Copper probes (five in this case) are placed in the ebonite insulator at these points - two large strips of copper, fastened to the ebonite at points corresponding to $r = r_c$ and $r = r_a$ are, of course, the electrodes. An arrangement of this nature is to be seen in Plate 1.

Outside the tank, electrical circuitry is provided so that the cathode-anode voltage is across a voltage dividing circuit of six equal resistors. The voltage at each point of the divider represents the desired voltage at each successive probe in the tank. These two voltages may be compared either with a vacuum tube voltmeter or, as was done in this case, their difference may be fed to the vertical deflection plate of a cathode ray oscilloscope. The electrode shapes are then adjusted until no signal is detected on the oscilloscope for any of the five probes. A motor drive was used which presented the voltage difference at each probe in turn to the oscilloscope. The horizontal deflection of the oscilloscope was provided from a potentiometer connected to the shaft of the same motor. The motor and cathode ray oscilloscope may be seen in Plate 2.

## 2.2. The Vacuum System.

The vacuum system used for the experimental work consisted

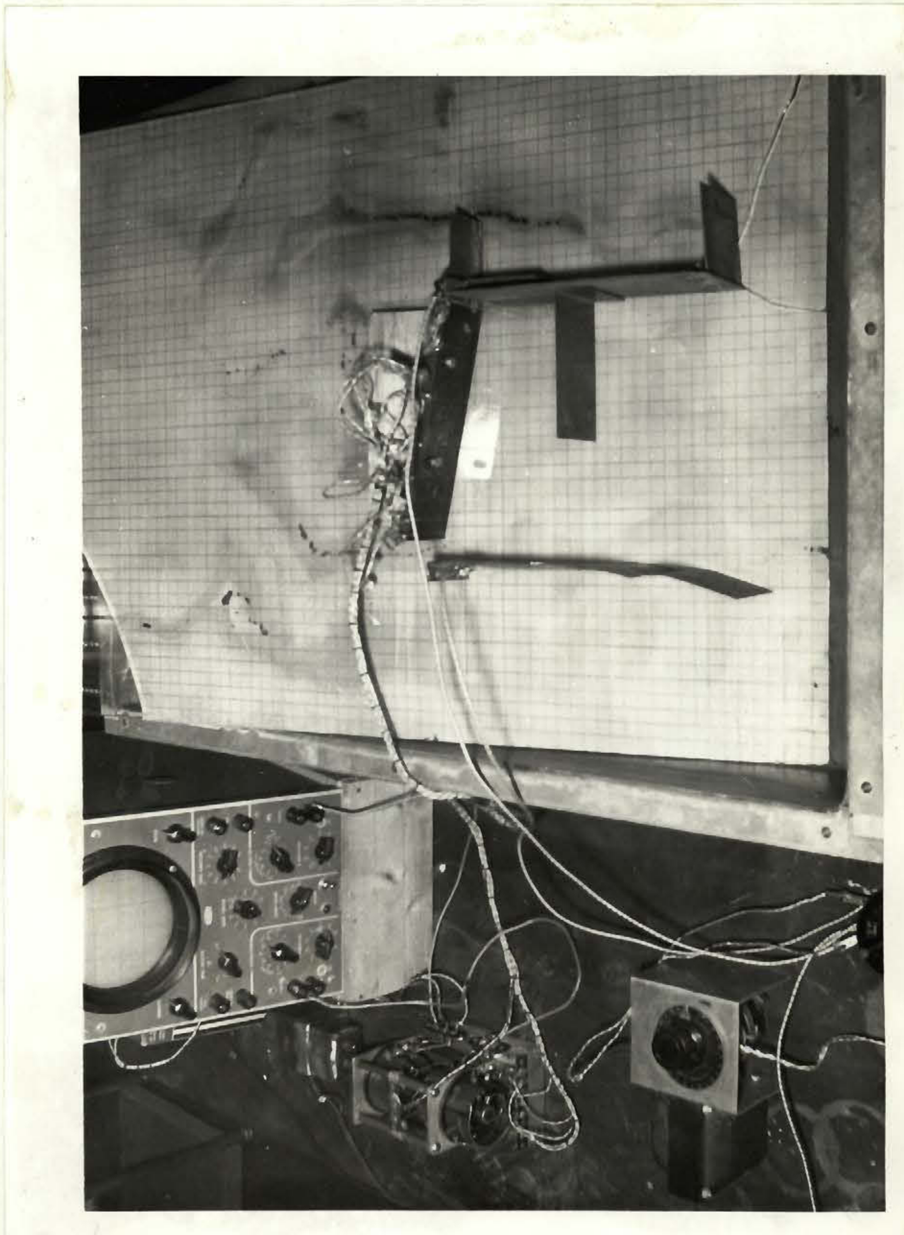

of a "Welsh" mechanical forepump, nominally capable of maintaining an ultimate forepressure of one-tenth of a micron, in series with a three-stage water-cooled oil diffusion pump. The oil used was silicone - in preference to "Octoil-S" which was thought to be injurious to oxide cathodes. A photograph of this equipment is seen, under the pump table, in Plate 3.

The forepump line was fitted with a "VG 1-A" type vacuum gauge while the high vacuum side was equipped with an ionization gauge of the laboratory's own make.

Between the diffusion pump and the gun structure under test can be seen a large silvered bulb. This is the thermos-type reservoir for the liquid-"air" "cold-trap". The surface area of the "cold-trap" exposed to the vacuum system remains constant as long as there is some liquid nitrogen in the reservoir. The reservoir when full, a volume of two litres, holds the nitrogen for 8 hours. The "heat" loss is mainly due to a glass join which is at the temperature of liquid nitrogen and exposed to air without any insulation whatever. However, the reservoir could conveniently be refilled every eight hours while experimental work was in progress, this being necessary, of course, since the system was in continuous operation.

The pressure obtainable with the glass parts of the system "sealed off" is $3 \times 10^{-7}$ mm.Hg. with no liquid nitrogen and $2 \times 10^{-8}$ mm.Hg. with liquid nitrogen. With the metal system connected and the gun filament at operating temperatures the

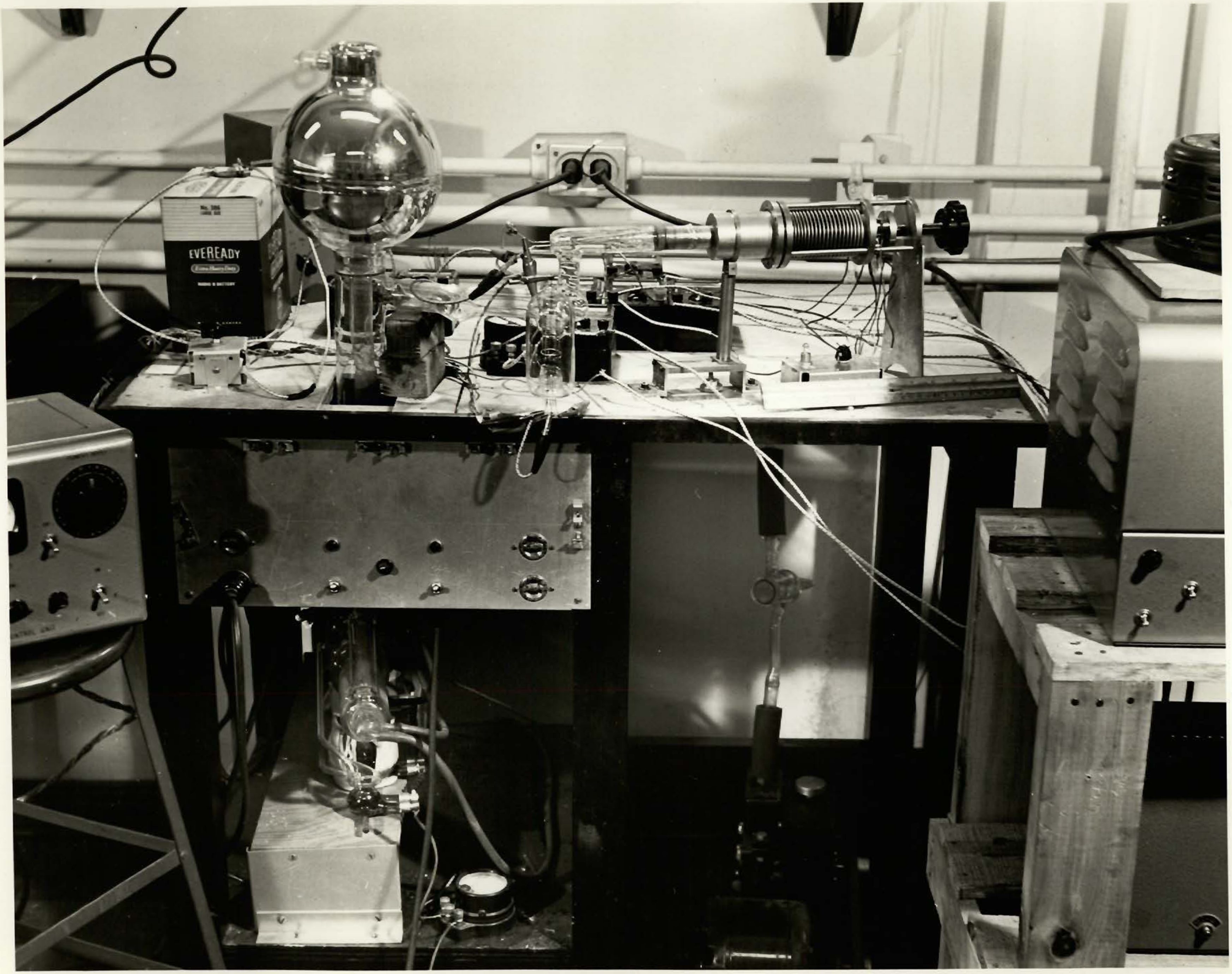


Plate 3

ultimate pressure is 2 x $10^{-7}$ mm.Hg.

In practice, with the electron gun in the system, the diffusion pump was not turned on until liquid nitrogen was in the cold trap. This ensured, to a great extent, that no oil vapour was present near the oxide cathode in the gun.

## 2.3. The Oxide Coating.

Previous Pierce type guns made at the Eaton Laboratory had utilised tungsten filaments (heated by passing current through them) as the electron emitters. They have the advantage of a relatively low power requirement and do not suffer from exposure to air between experimental runs. However, the filament does not, by any means, constitute a uniform source of electrons - a requirement that is assumed in the theoretical development of Pierce guns. In addition, it has been shown (2) that the electric fields which exist along the filaments adversely affect the performance of the gun.

With an indirectly heated oxide cathode, the power required is greater, but the emission is much more uniform than with a filament. The emitter may also be held at one potential (i.e. zero) eliminating the electric fields accompanying the filament. Oxide cathodes however, once activated, cannot be exposed to air and are sensitive to positive ion bombardment. The advantages of oxide cathodes outweigh their disadvantages in the author's mind and they were used in the guns tested.

The base metal for the cathodes was "225 active" nickel, which was prepared for spraying in the following manner.[4]

(1) Agitate in Acetone.

(2) Boil in the following solution for five minutes.

| | | |
|---|---|---|
| Sodium Carbonate | ... | 40 grams/litre. |
| Sodium Hydroxide | ... | 13 grams/litre. |
| Sodium Cyanide | ... | 13 grams/litre. |

(3) Boil five minutes in distilled water.

(4) Rinse in 5% warm acetic acid.

(5) Agitate in three changes of boiling distilled water.

(6) Rinse in clean methyl alcohol.

(7) Dry in air.

(8) Fire in hydrogen at 900° C.

(9) Spray oxide-coating.

If for some reason there is a time lapse between the hydrogen firing and the spraying, the nickel should be stored in an evacuated dessicating jar.

The oxide-coating material is obtained from Raytheon Manufacturing Company, Newton, Mass. under the designation C-51-2. Just previous to spraying, the mixture is rolled for one hour in a half-gallon bottle in the glass lathe. The coating is applied to the cathode surface with a spray gun of the De Vilbiss CH type. In use the fluid screw is set about half to three-quarter turn, and the spreader valve adjustment is made "zero". Compressed nitrogen was used in preference to compressed air, at a pressure of 14 pounds, with the gun operating. Before

(1) The material is first cleaned to reduce surface contaminents. An electrolytic etch of sulphuric acid, buffered by boric acid to saturation, is used at room temperature. The part being cleaned is made the anode and treatment times of 3 minutes are satisfactory.

(2) The parts are rinsed in clean running water.

(3) A rinse in 20% hydrochloric acid at room temperature is followed by a water rinse.

(4) The parts are then electroplated in a chloride bath of the following composition:

Nickelous chloride ... 32 grams.
Hydrochloric acid (conc.)..500 cc.
Water to make one gallon.

The activation of the alloy surface is apparently effected through the bombardment of the metal by atomic hydrogen - with a tightly bonded nickel film being deposited at the same time. This "strike" is used for 3 minutes at 3 volts d.c.

(5) Parts are rinsed in clean running water.

(6) The parts are transferred to a Standard Watts solution and plated to the required thickness.

This solution will plate at the rate of 0.0001 inch per minute at 125 amperes per square foot at room temperature. For protection against oxide film formation on chromium alloys during treatment at high temperatures the thickness of the electrodeposit will vary directly with temperature and treating time. For firing temperatures up to 1200 degrees centigrade and treating times up to sixty minutes, a thickness of nickel of .001 inch is sufficient. At 900° C the nickel at the interface begins to alloy with the base metal producing a tenacious protecting surface.

(7) After nickel plating the parts are rinsed and flash copper-plated for 90 seconds at 25 amperes per square foot in a Rochelle-salt copper cyanide plating bath.

| | | |
|---|---|---|
| Copper cyanide | ... ... | 12.2 grams/litre. |
| Sodium cyanide | ... ... | 16.1 grams/litre |
| Sodium carbonate | ... ... | 15.2 grams/litre |
| Potassium sodium tartrate (Rochelle salt) | .. | 15.2 grams/litre |

(8) A water rinse and a dip in 5 - 10% sulphuric acid ensures a cyanide free surface.

(9) The parts may then be dried in air after an alcohol and acetone rinse.

The plated stainless steel may now be safely hydrogen fired at 900° C.

## 2.5. Gun Testing Circuit.

Two modified Pierce guns were designed for use with 3 mm. oxide cathodes made in this laboratory. The author designed one gun for the experimental work to be described here while the other was intended for use by another graduate student.(5) Although the former gun was intended for use in the beam testing device described in the following section, its performance and properties were tested in a separate experimental set-up.

The gun was mounted onto a glass base as shown in Plate 4, and sealed into the vacuum system. It was intended that the gun be tested over the range zero to 1500 volts for perveance and partition. In addition it was desired to see if the beam shape was approximate to the design value - merely to provide a foretaste of the more exact measurements to be performed later. For this purpose an apertured plate was placed at the calculated position of the beam minimum, the aperture diameter being the calculated size of the beam diameter at this point. Behind this aperture was a small collector. It was possible to measure the separate currents to the gun anode, apertured plate and collector, as may be seen from Figure 12. In this way the total current, hence gun perveance, and partition could be measured; and the fraction of the beam current received by the collector gave some indication of the validity of the theoretical prediction of beam size.

Not shown in the diagram of the gun circuit is the fact that the collector was made slightly positive with respect to the apertured plate to prevent secondary emission from the collector to the plate.

The cathode electrode was biased negatively with respect to the cathode, the extent of the bias being varied by means of a rheostat. Because of the physical proximity of the cathode electrode and anode (they are separated by a small lavite spacer) and their potential difference, a leakage current existed between

Figure 12: Gun Testing Circuit

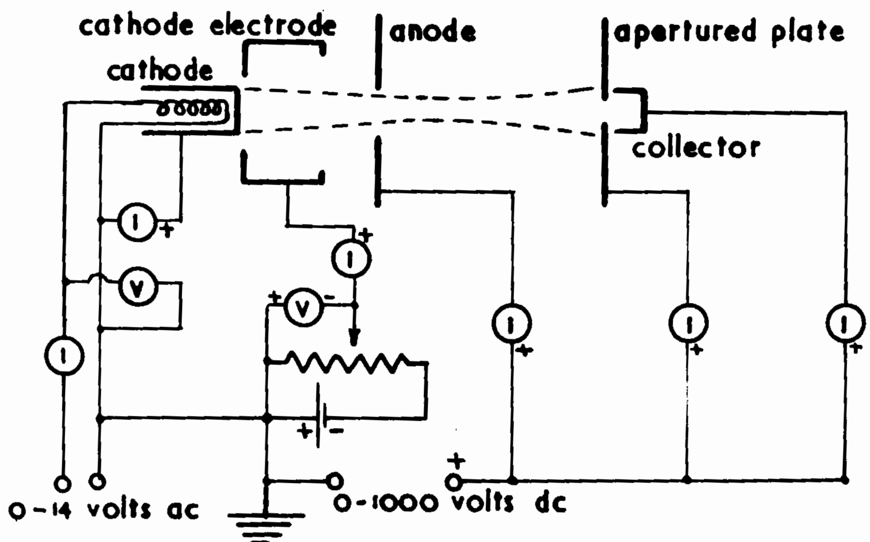

A compressible berrylium-bronze bellows was decided upon, and provided a longitudinal motion along the beam of one inch. A drawing of the beam testing device is shown in Figure 13, while a photograph of it on the vacuum system is shown in Plate 5.

The transition from the glass vacuum system to the metal beam testing device was effected by means of a glass-kovar seal. The kovar was then "soft-soldered" to the stainless steel.

The electron gun was designed so that the cathode, cathode electrode and a lavite spacer could all be seated and held inside the anode. The gun was then a compact unit and could be slid to a seated position in the beam testing device, where the gun leads could be sealed through the glass of the vacuum system (see Figure 13). In front of the gun, and a sliding fit inside the gun housing, was a many apertured plate (Plate 8). Behind each aperture was a separate collector, all the collectors being held in a lavite disc which mounted in the apertured plate. Leads to the individual collectors were brought out of the vacuum through glass by means of another glass-kovar seal.

The apertured plate itself was connected by three nickel-plated brass rods to a plate on the back end of the bellows. In this latter plate was also the glass-kovar piece; and thus this marks the boundary of the vacuum system. The front end of the bellows, fitted with a brass flange, was held, by the air pressure, against a similar flange on the gun housing. To ensure a vacuum tight seal, a rubber "O" ring was between these two flanges.

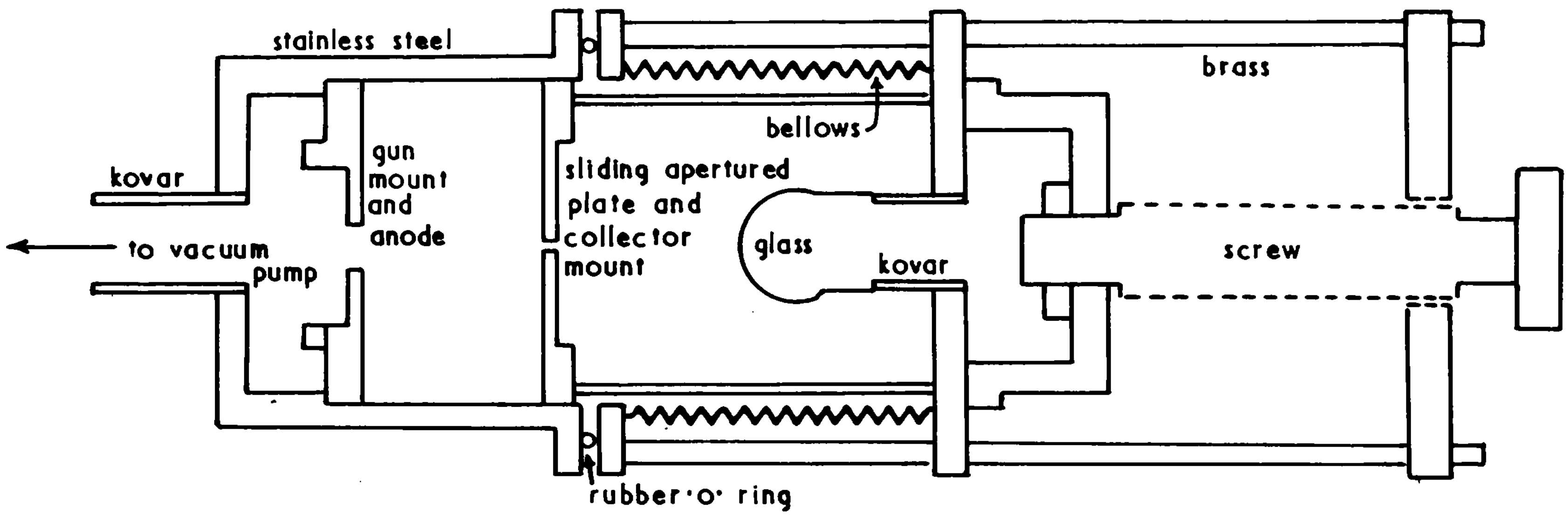


Figure 13: Sketch of Beam Testing Apparatus

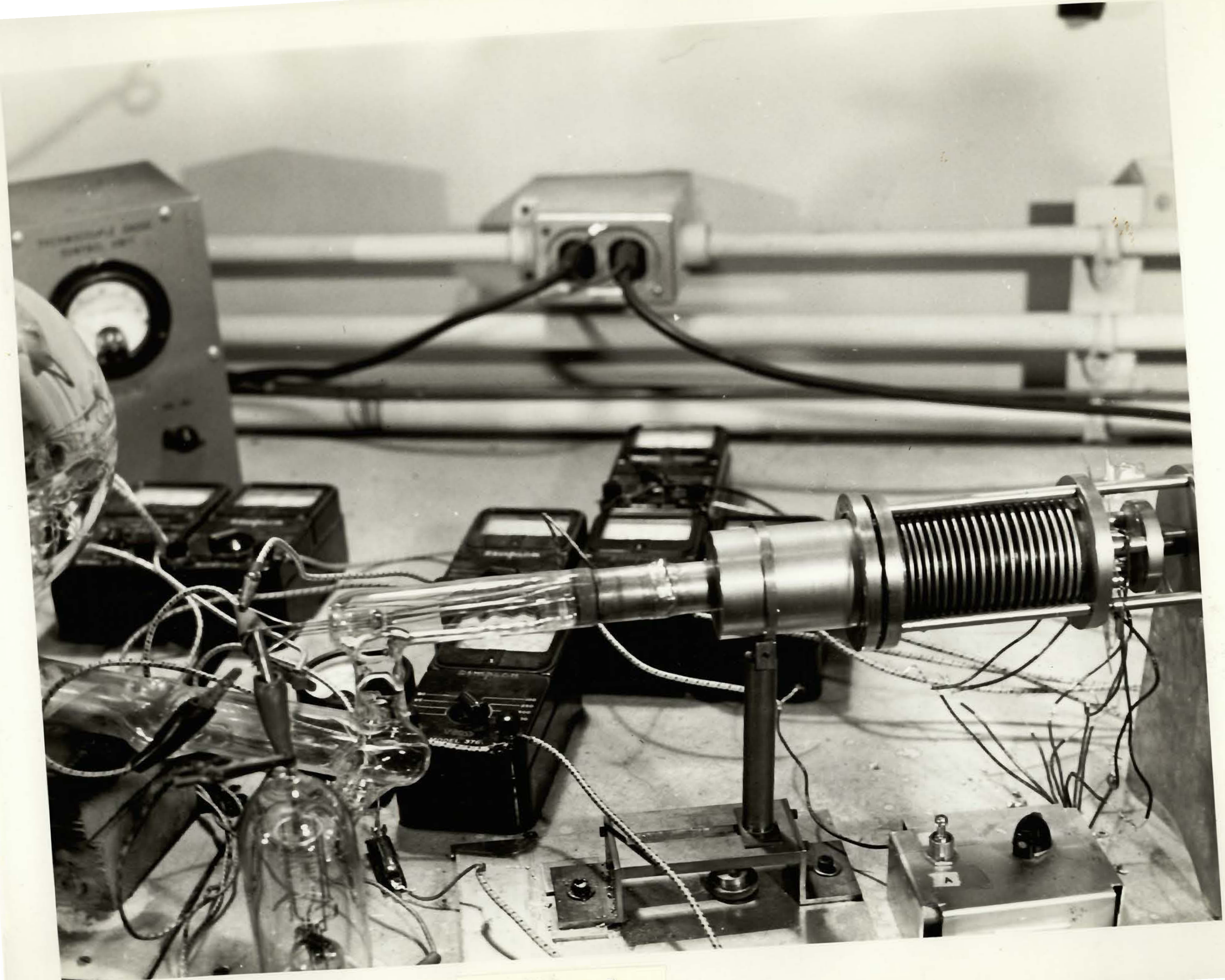

Plate 5

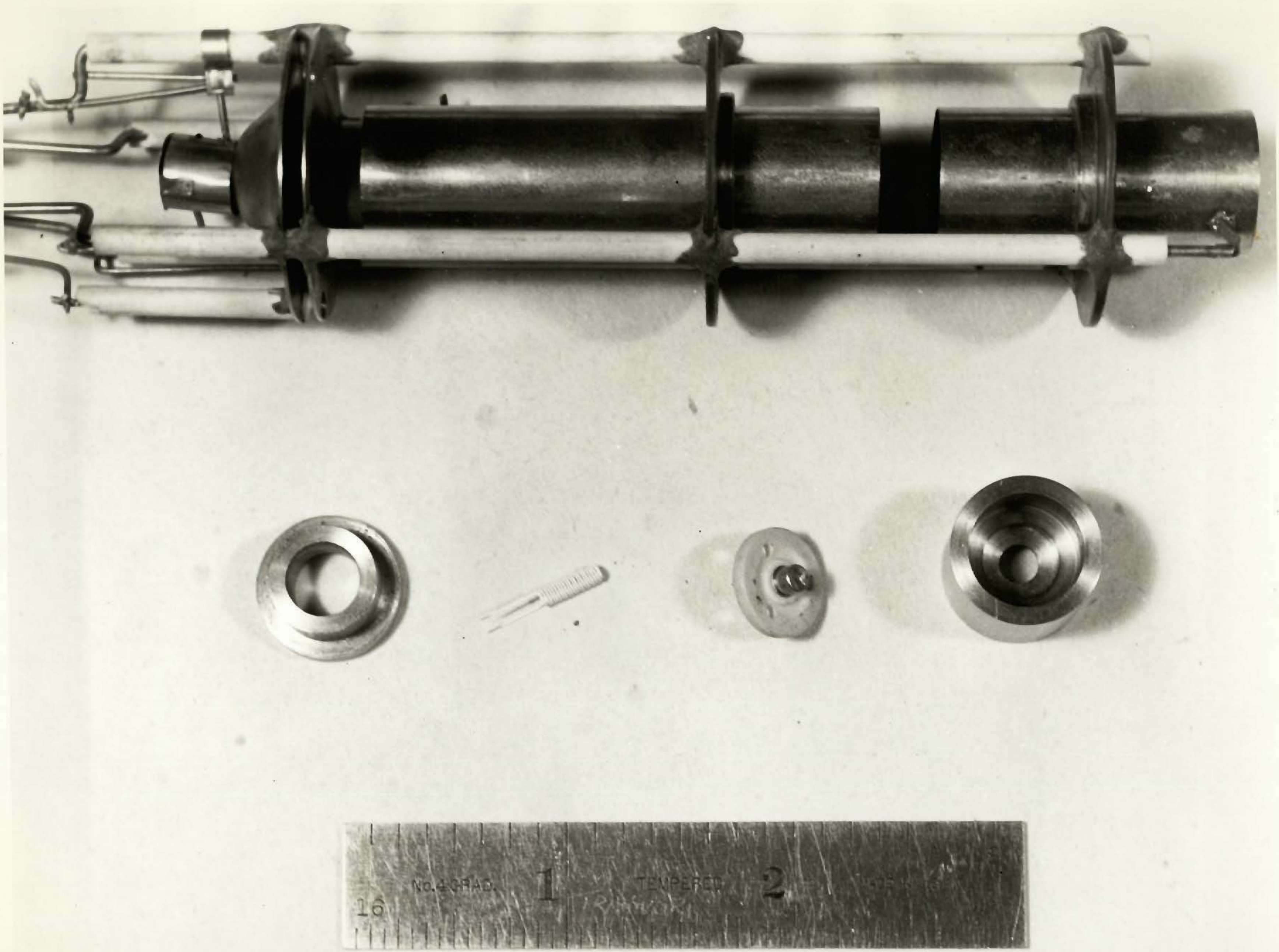


Plate 6

By turning the main screw appropriately the bellows could be extended or compressed, moving the apertured plate and the collectors longitudinally in the gun housing. Within machining limits, the alignment between gun and apertured collectors can be maintained during the motion.

The vacuum pressure obtained in the system with the cathode at operating temperature was $2 \times 10^{-7}$ mm.Hg. A fan was used to cool the gun housing during operation.

## 2.7. Beam Testing Circuit.

This circuit was, of course, very similar to the gun testing circuit shown in Figure 12. Here however the anode, gun housing and apertured plate are all in physical contact and the currents to them could not be measured separately. Again the collectors were made positive with respect to the apertured plate, to prevent secondary emission, while a switch enabled the measurement of the current to the various collectors by one micro-ammeter.

## 3. RESULTS.

### 3.1. The Electrode Shapes.

The Pierce guns hitherto used in this laboratory used the "exact" Pierce shapes as determined in an electrolytic tank. The shapes were, as stated previously, spherically symmetrical, but curved. In order to manufacture these electrodes a photograph was taken of the shapes in the tank and the negative suitably enlarged to the desired actual electrode size. From this negative a die was made in the workshop, and electrodes could easily be punched out.

The cathode and anode electrodes were aligned with one another by means of alundum rods passing through location holes previously punched in the electrodes. Alignment was facilitated by the use of a jig. The emitter was then mounted behind the aperture in the cathode electrode and supported there by the alundum rods. A gun built by this procedure is shown at the top of Plate 6. The cylindrical electrodes shown following the gun are merely for electrostatically focussing the beam and are not an integral part of the gun.

It was desired to design and build a gun in which the electrode shapes could be more accurately and easily made and in which the alignment procedure would be simplified.

It was possible to obtain an approximate solution to the space charge problem in the electrolytic tank with straight-line electrode shapes. The solution is "approximate" inasmuch as the voltages along the beam edge were all within 2% of their proper value. The cathode electrode is shown in Figure 14 and it is biased negatively with respect to the cathode. The anode shape is merely a disc with an aperture equal in size to the cathode electrode aperture. Both these electrodes can be accurately turned out on a machinist's lathe.

The cathode electrode was also built so as to receive the actual cathode, mounted in a lavite ring, and a cathode retaining ring shown in Figure 14(a). The various components of the gun, except for the anode, are shown at the bottom of Plate 6. Each component in turn fits into the other: the cathode fits into the cathode electrode and is held in position by the retaining ring; this unit then fits into a lavite spacer which positions it inside the anode disc. The gun is then a single, compact self-aligning unit. The cathode electrode with the cathode mounted in it may be seen in Plate 7 while the entire gun, with a collector in front of it, is shown in Plate 4.

There is an additional advantage to the gun configuration determined, which is by no means insignificant. In the former type of Pierce gun the cathode and cathode electrode are maintained at the same potential, usually zero. Theoretically the zero equipotential must leave the cathode edge at an angle of $67.5^{\circ}$, but in practice the hot cathode and cathode electrode cannot be held in physical contact, and the slight displacement of one relative to the other causes a violation of the condition for the angle of the zero equipotential. Cutler and Saloon[7] show that, for their gun at 1000 volts anode potential, a

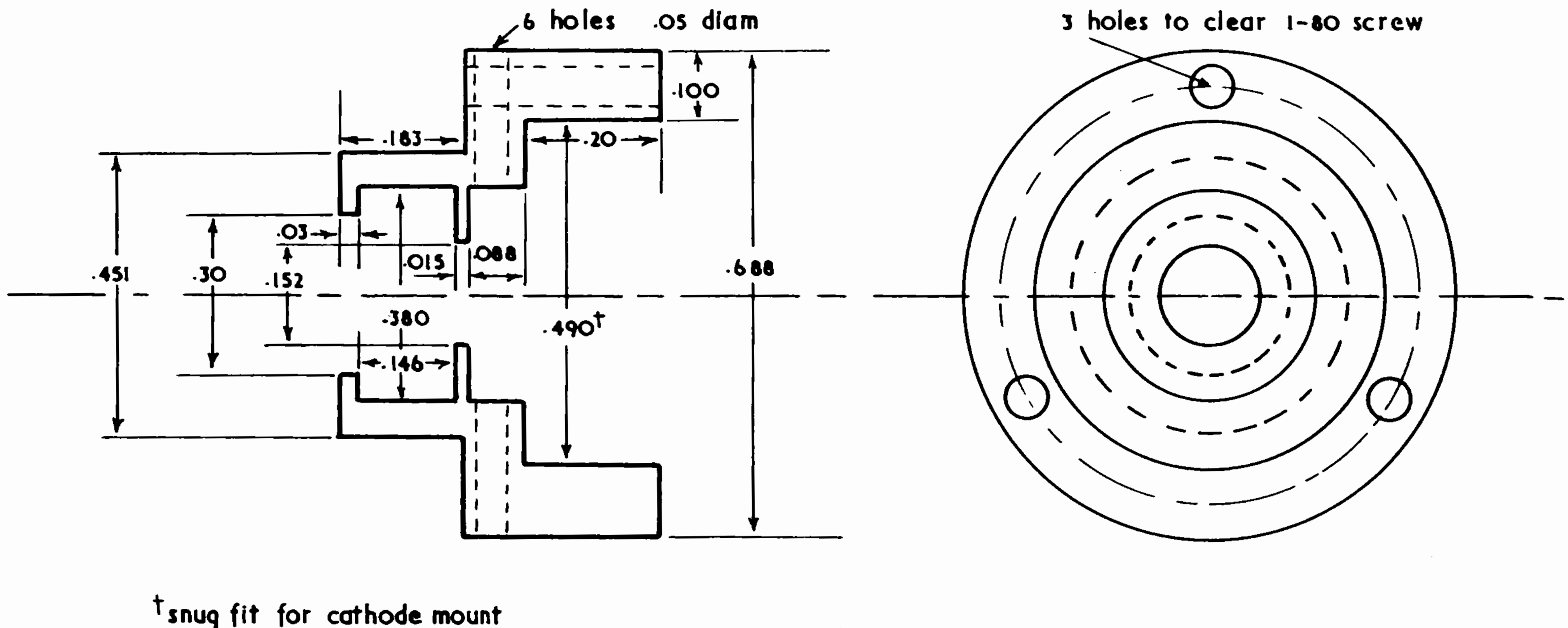


Figure 14: Cathode Electrode

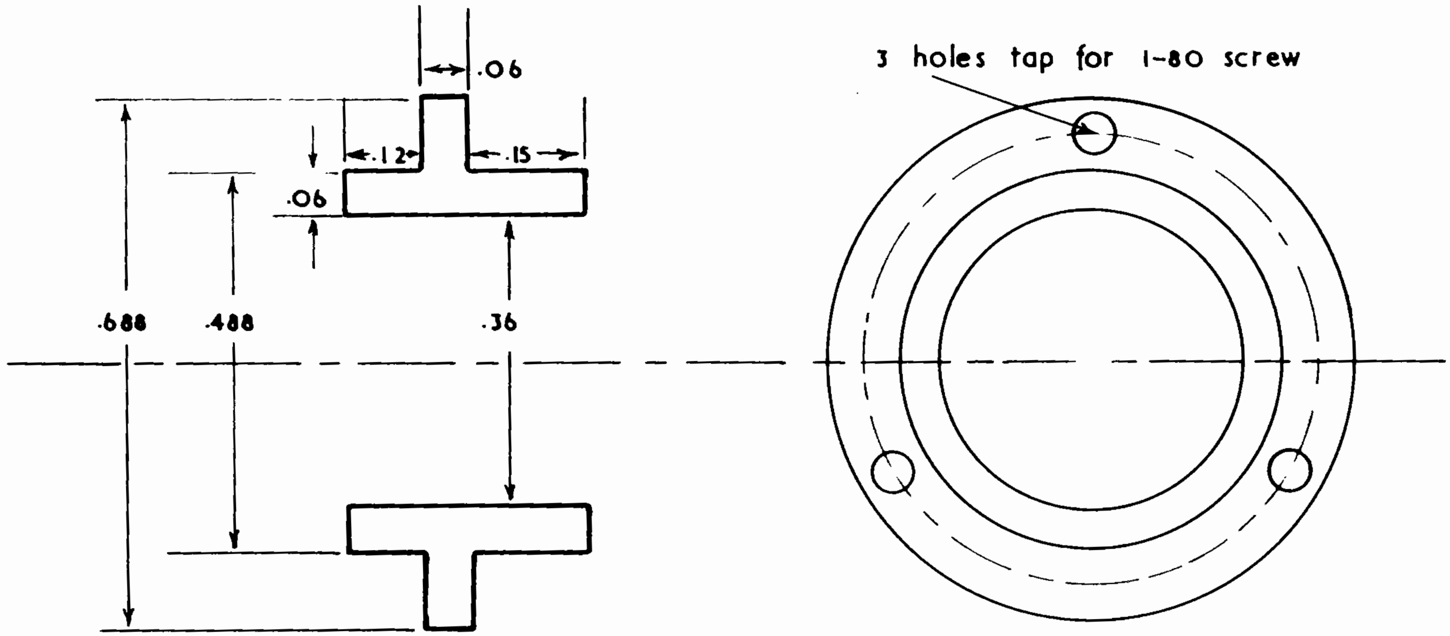


material stainless steel
scale 4 x full size

Figure 14(a): Heat Shield & Retaining Ring

Plate 7

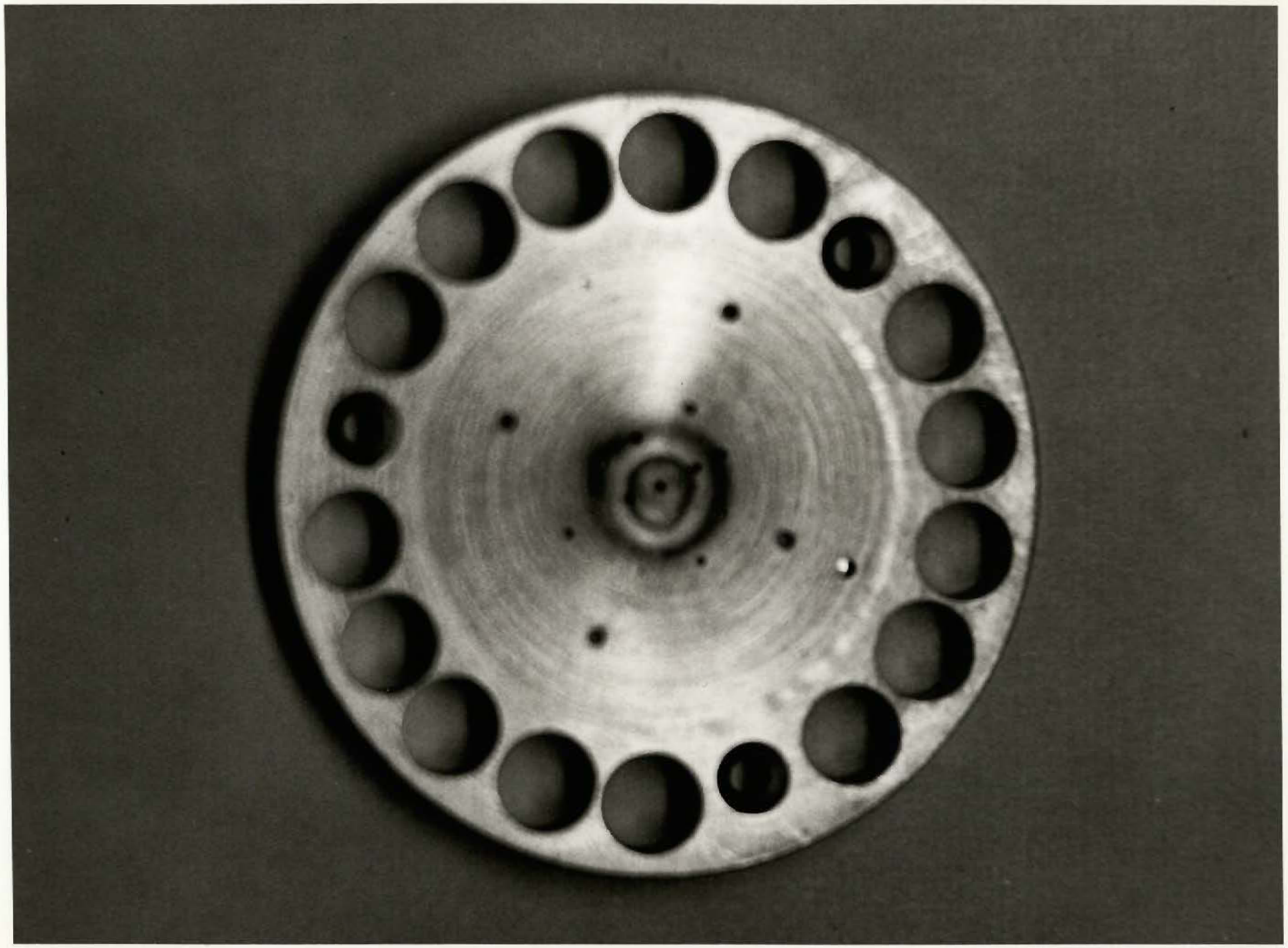

Plate 8

displacement of the cathode of 0.002 inches results in an effective error of 1.2 volts, causing an excess of transverse electron velocities in the beam.

In the present design, however, the zero equipotential is effectively "simulated", by the negatively biased cathode electrode, and it may be made to satisfy the proper conditions right up to the cathode edge.

Another relatively unsatisfactory aspect of Pierce gun theory is the assumption of the thin lens formula for the action of the anode aperture. This approximation becomes noticeably poor for large angles of convergence ($\theta$) and when the anode aperture compares in size with the cathode-anode spacing.

In the design of the present gun, the effect of the anode aperture was determined in the electrolytic tank. A distinction was drawn between the accelerating or anode electrode and the "effective anode". The electrode shapes are such that the voltage variation as in Equation (1) is maintained up to the "effective anode" only. Beyond this, the equipotentials were plotted as in Figure 15. The effect of the region from the "effective anode" through to the anode aperture and beyond until the drift space was calculated by simple electrodynamics. From the equipotential shapes, it was judged that the beam would only "see" a longitudinal electric field (the curvature of the equipotentials being slight) until it had left the gun region, and the effect of this field on beam shape is easily calculated. The calculations (which include the effect of thermal velocities) were used to predict

# Figure 15: Gun Aperture Equipotentials

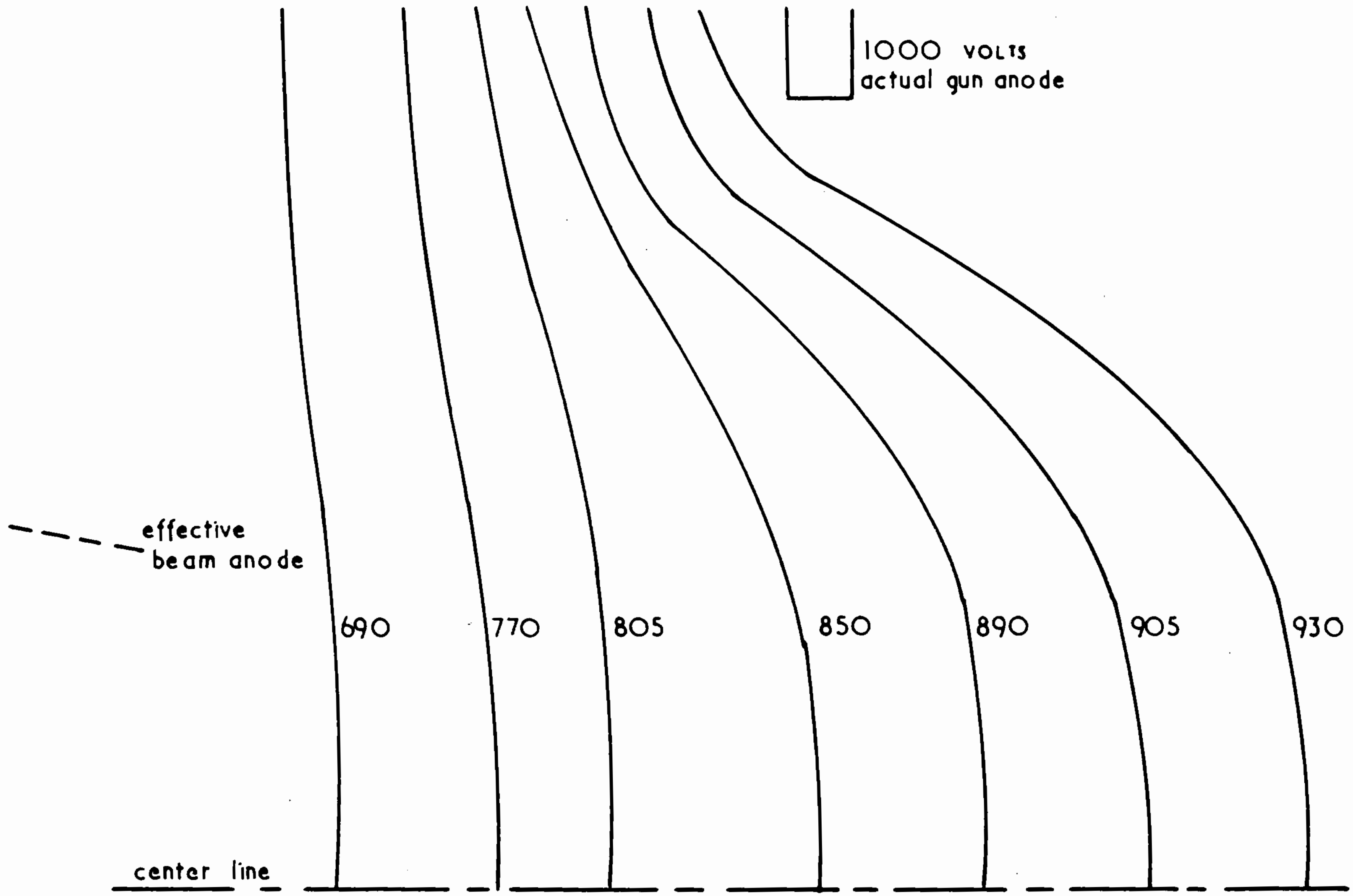


scale 80 x full size

beam radius outside the gun and were experimentally checked. Thus the necessity of using the aperture lens formula was eliminated by a more detailed, but simple consideration of the actual fields present.

3.2. Gun Performance.

The Pierce gun designed had a ten-degree angle of convergence and a design perveance of 3.32 milliamperes per kilovolt. The gun was first tested with a stationary apertured plate and collector placed at the beam minimum as calculated using the above considerations. The aperture was made the size of the calculated beam radius and the arrangement is sketched in Figure 12. A photograph of the gun appears in Plate 4.

The gun was operated at a pressure of less than $2 \times 10^{-7}$ mm.Hg. below 1200 volts on the anode. Above this voltage the beam current ($\sim$ 6 mA) caused severe outgassing of the collector and the pressure rose to $10^{-6}$ mm.

Graph 1, curve (a) shows the variation of beam perveance with anode voltage. There is very little variation in perveance over the entire range in voltage. The average perveance is 3.60 mA/kV $^{3/2}$, as compared with a theoretical one of 3.32 mA/kV $^{3/2}$, the experimental value being 8.5% higher. It must be realised that any positive ion current would contribute to measured electron current and thus tend to raise the measured perveance. This phenomenon could, in fact, be observed experimentally. On drawing a particularly heavy gun current, the first effect of the outgassing is to increase the measured beam current, then as the emissive coating is poisoned by positive ions, the beam current drops to a lower value than initially.

Graph 1, curve (b) shows the measured beam current as a function of anode voltage. It does not deviate more than 0.25 mA from the expected beam current.

In Graph 2 is plotted the percentage of the beam current which reached the collector. The aperture in front of the collector was the same size as the calculated beam radius, and if the assumptions concerning the fields inside the gun were correct 98% of the beam current should have reached the collector. The figure "98%" is quoted since Cutler and Hines Thermal Velocity theory was used, and this enables the prediction of beam radius enclosing various fractions of the total beam current.

The current actually reaching the collector was between 91% and 96%. This is considered to be good evidence of a fairly accurate means of predicting beam radius.

Graph 3 shows the Gun Partition as a function of anode voltage. It was essentially 100% over the entire range of voltage used - a very satisfactory result.

In Graphs 4 - 7 is shown the variations in cathode current and collector current (as a percentage of total) with cathode electrode bias voltages, taken at several anode voltages. The curves of collector current illustrate how the bias virtually "focusses" the beam - there being an optimum bias at each anode voltage. The value of this voltage was in all cases quite close to that of the design bias - a constant fraction of the cathode anode voltage. The variation in cathode current shows that the cathode electrode may also be used as a "grid" - to provide a control for the cathode current at any particular anode voltage.

At an anode voltage of 1500 volts the current density at the collector was 200 milliamperes per square centimeter, whereas the current density at the cathode is approximately 90 milliamperes per square centimeter.

3.3. Beam Measurements.

The beam data was obtained by the measurement of the current received by several apertured collectors which were moved along the beam length (plate 8). The total longitudinal motion used was one inch. Experimentally, however, the collector at the center of the beam received the only measurable current. There was a minimum radius at which the off-center apertures could be placed. The beam spread was usually not great enough, and the current density at these radii too low, to provide measurable current to these off-center holes.

Using thermal velocity and space charge spreading theory, the variation in current density at the center of a particular beam can be predicted. It was thus possible, with the experimental information obtained, to compare the actual beam spreading, with the spread expected due to space charge and thermal considerations.

The current density at the center of the beam ($J_c$) relative to that at the anode ($J_a$), was plotted against anode distance. Graphs 8 to 12 show this data for beams ranging from 200 to 1000 volts. The bias voltage on the cathode electrode was zero for all these beams and the perveance thus varied considerably as the anode voltage was changed.

The three curves presented on each graph are: the beam spreading predicted by space charge alone, by space charge and thermal velocity theory, and the experimental curve.

The 200 volt beam spreads in a manner quite close to the thermal theory. It is to be expected that the experimental curve should spread less than as given by the theory of Cutler and Hines for they predict the upper limit of the spread. In addition, any positive ions would partly neutralise the space charge and thus reduce the spreading. The experimental curve does not possess a maximum as does the space charge spreading curve. In the case of the space charge curve the maximum would indicate the position of the minimum beam radius - for the theory used to derive the curve assumed a uniform current density. In the experimental, or thermal, curve, a maximum of J center/J anode does not indicate the position of the beam minimum; for the current density is by no means uniform throughout the beam, and the maximum current density at the center need not occur at the beam minimum.

At 600 volts (Graph 10) the experimental curve is still similar to the theoretical thermal curve and exhibits a maximum quite close to the position of the theoretical maximum. It is not to be inferred from these curves however that the experimental current density is higher than the space charge current density at this maximum, for these curves are both relative to the density at the anode which, in the case of the space charge curve, is higher than that for the experimental curve.

In a given distance, thermal velocity spreading is less severe at the higher beam voltages, for it has less time to make itself felt. At the higher voltages (Graphs 11, 12) the beam spreading was reduced even more so than would be expected. In addition, the maximum was found further from the anode than expected. This increased divergence between the experimental and thermal spreading curves is most probably due to positive ions. The outgassing of the apertured plate and collector caused the pressure to rise at these voltages (from $3 \times 10^{-7}$ to $10^{-6}$ mm.Hg.) and the consequent positive ion neutralisation would reduce beam spreading due to space charge. Also, by effectively "lowering" the perveance of the beam the minimum would be "pushed" further from the anode.

Additional curves of J center/J anode are found in Graphs 13 - 15. These were taken with the cathode electrode properly biased and the curves are very similar to the previous ones.

Assuming that the theory of Cutler and Hines applies, it is possible to convert these previous curves into beam profiles. This has been done by using the measured value of current density at the center of the beam, $J_c$, to calculate $J_c/J_a$. Using Figure 10(a) this enables the determination of $r_e/\sigma$ , which in turn, by virtue of Figure 11, determines the values of $r/\sigma$ for various enclosed values of beam current. Thus, knowing $\sigma$ , the beam radius may be calculated as a function of distance from the anode. Beam Profiles corresponding to Graphs 8 - 15 are shown in Graphs 16 - 23.

On these graphs one may observe visually the comparison between experimental and theoretical beam spreads. Again at the lower voltages is seen the close similarity in spreading between the two; positive ions, of course, lessening the similarity at the higher voltages. In addition, the beam minimum appears to be closer to the anode than predicted, by the space charge spreading curve; an observation made in the paper by Cutler and Hines.

Certain peculiarities of behaviour prompted a further series of tests. At two distinct anode voltages, the gun was operated in each of the following three states:

(a) proper cathode electrode bias, usual heater voltage.

(b) lowered cathode electrode bias, usual heater voltage.

(c) proper cathode electrode bias, reduced heater voltage.

In each of these states the current to the center collector, $I_c$, was measured as it was moved longitudinally along the beam. In Graphs 24, 25, the ratio of $I_c$ to the total current from the gun, $I_c$ A, is plotted against anode distance. Both graphs illustrate the same phenomena.

The effect of lowering the bias is to increase the total current emitted from the gun, but since curve (b) is lower than curve (a) it also has the effect of making the beam much more diffuse. Thus the focussing effect of the cathode bias is well illustrated here.

The lowering of the heater voltage drastically reduces the current from the gun. However, the current received by the center collector is higher with the lower heater voltage. This shows the beam to be much more dense with the lower heater voltage - a phenomenon which graphically illustrates that spreading is indeed due to thermal velocities. The extent of the spreading voltage is such that even though the total current is halved, by lowering the voltage, the center collector receives (relatively) three times as much current as when the heater voltage is at its usual value.

At the center of the 1000 volt beam the maximum current density is of the order of 250 milliamperes per square centimeter, while the average beam current density at the minimum is closer to 200 milliamperes per square centimeter.

# Graph 1

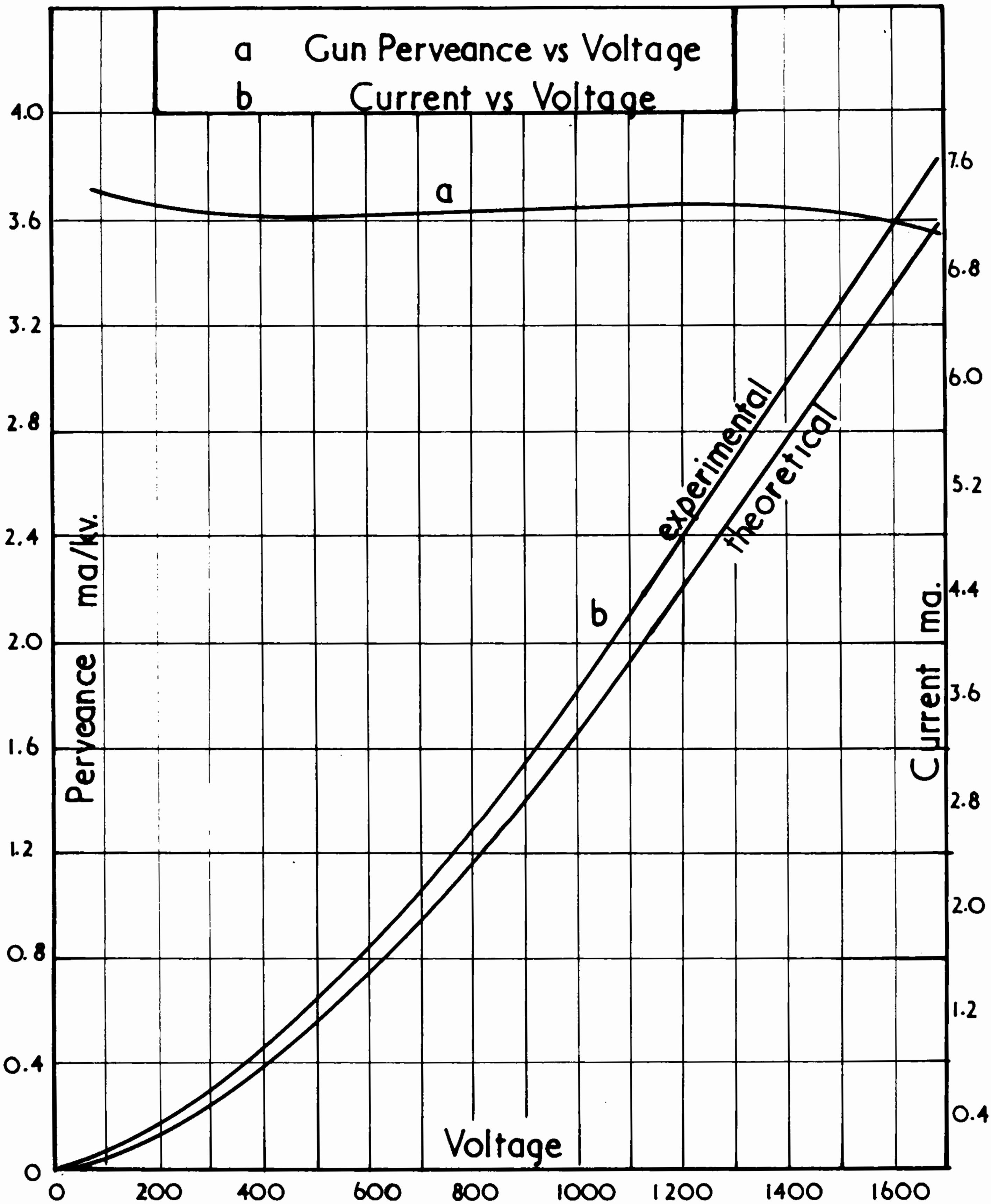
a Gun Perveance vs Voltage
b Current vs Voltage
a
b
experimental
theoretical
Perveance ma/kv.
Current ma.
Voltage
4.0
3.6
3.2
2.8
2.4
2.0
1.6
1.2
0.8
0.4
0
7.6
6.8
6.0
5.2
4.4
3.6
2.8
2.0
1.2
0.4
0
200
400
600
800
1000
1200
1400
1600

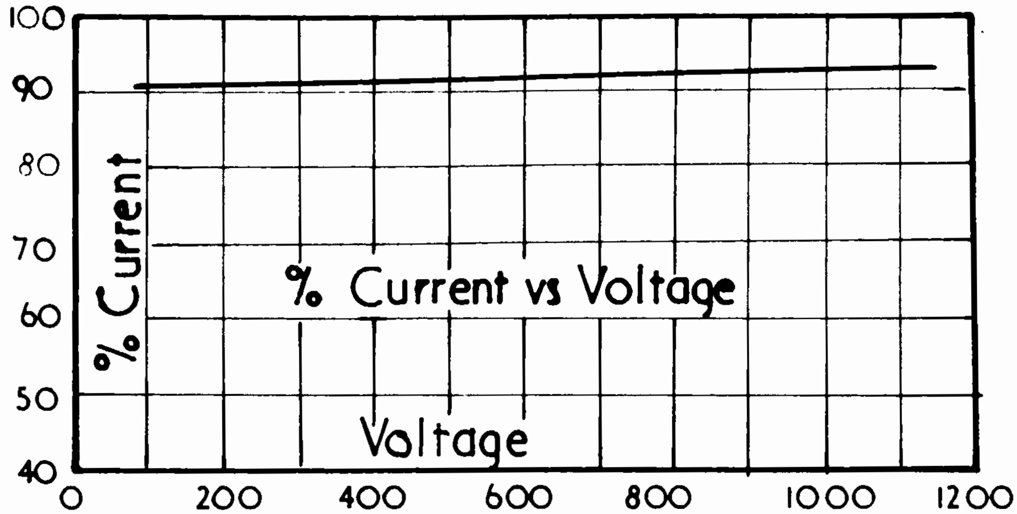


Graph 2

Graph 3

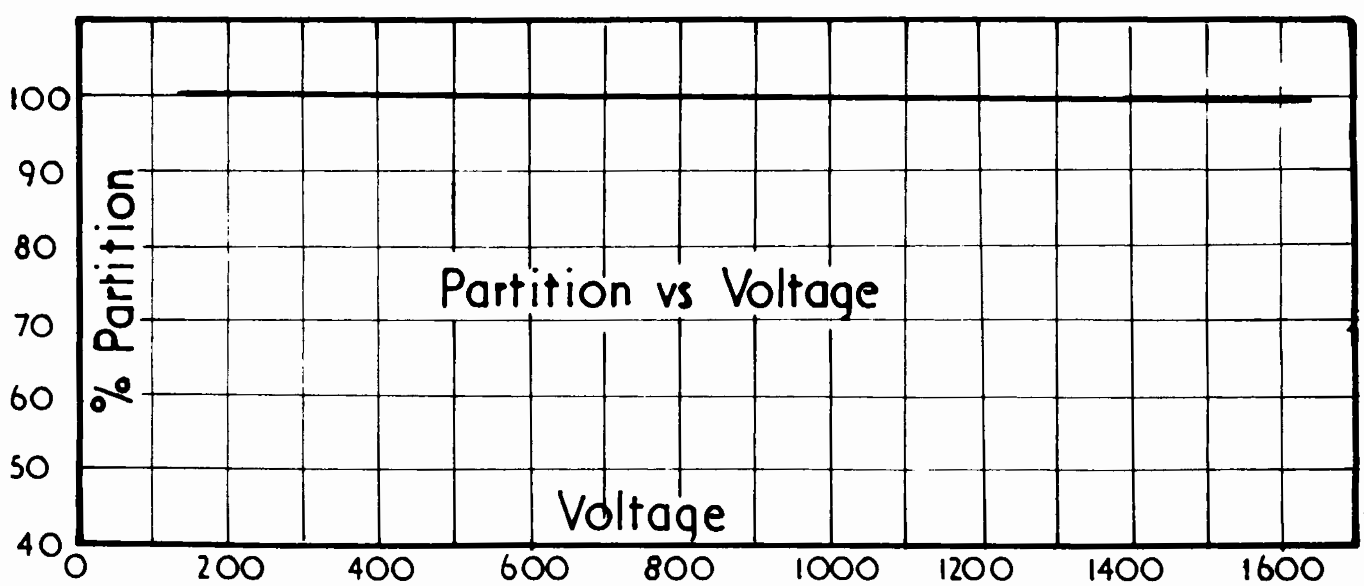

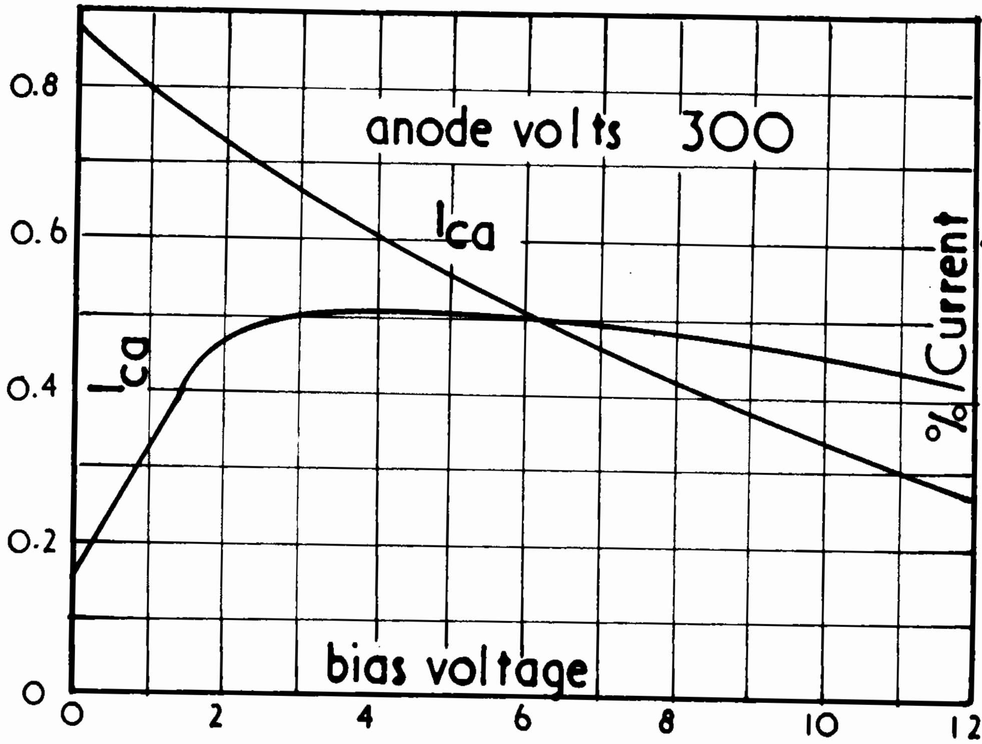


Graph 4

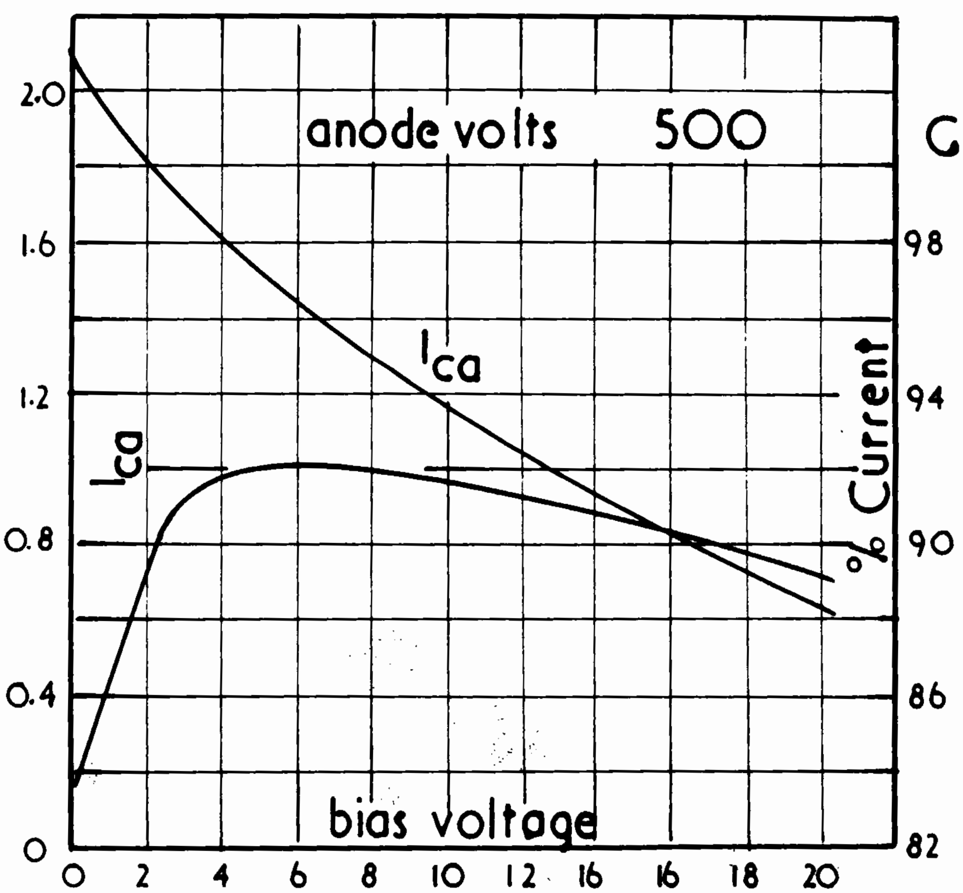


Graph 5

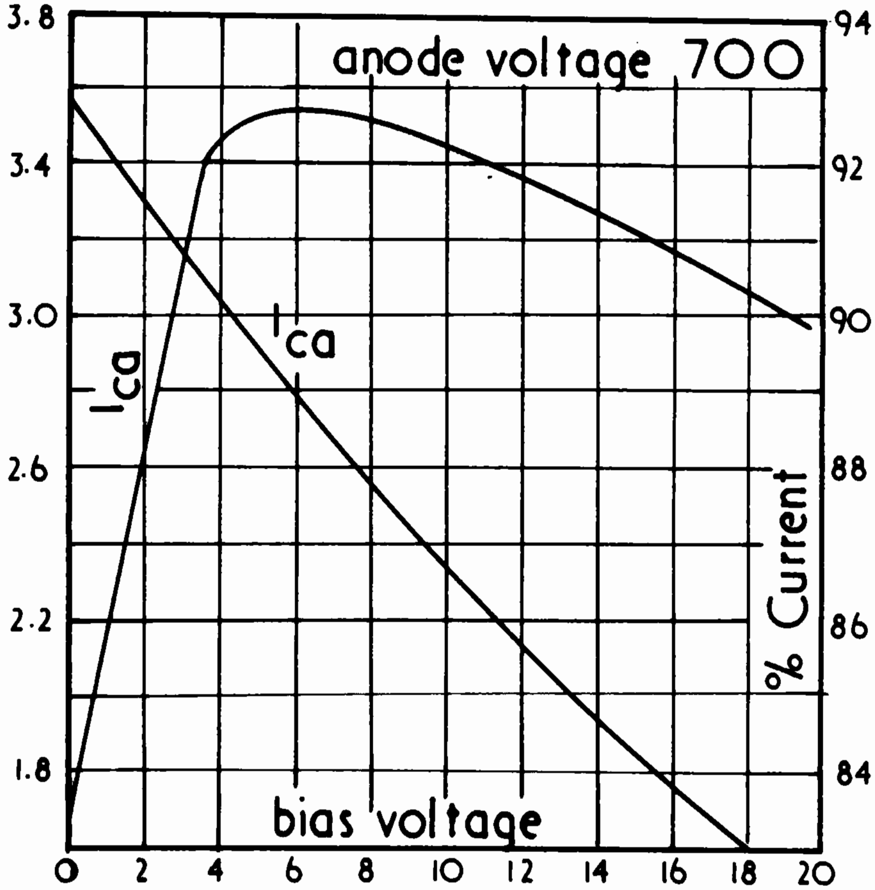


Graph 6

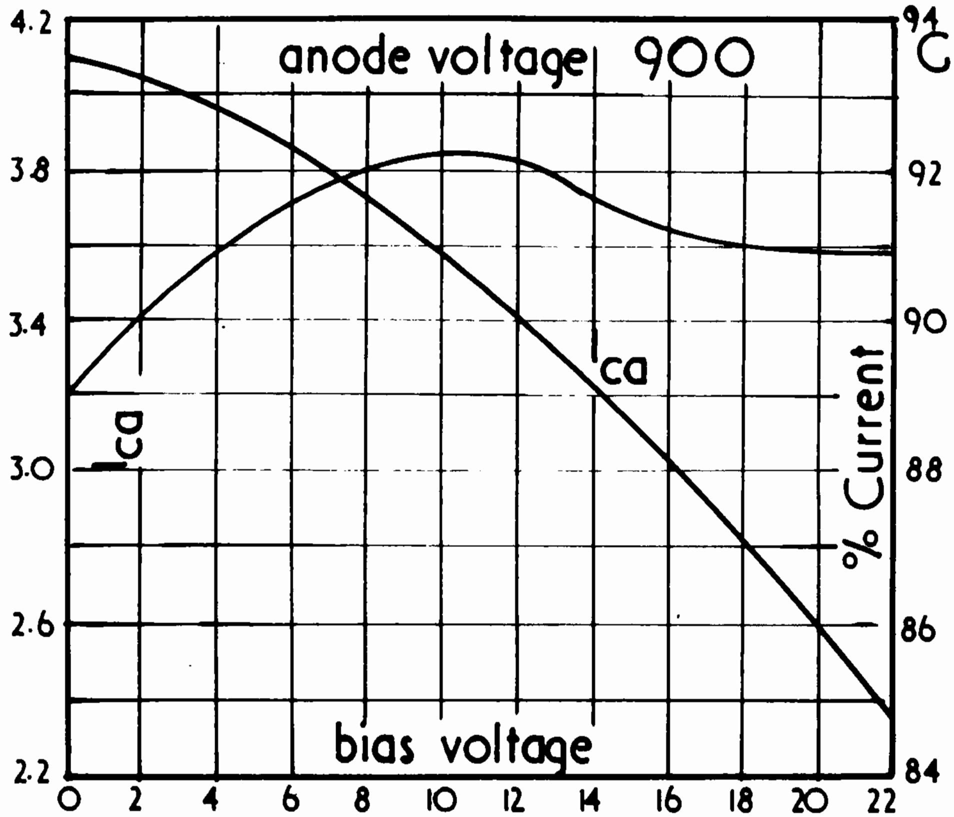


Graph 7

Graph 8

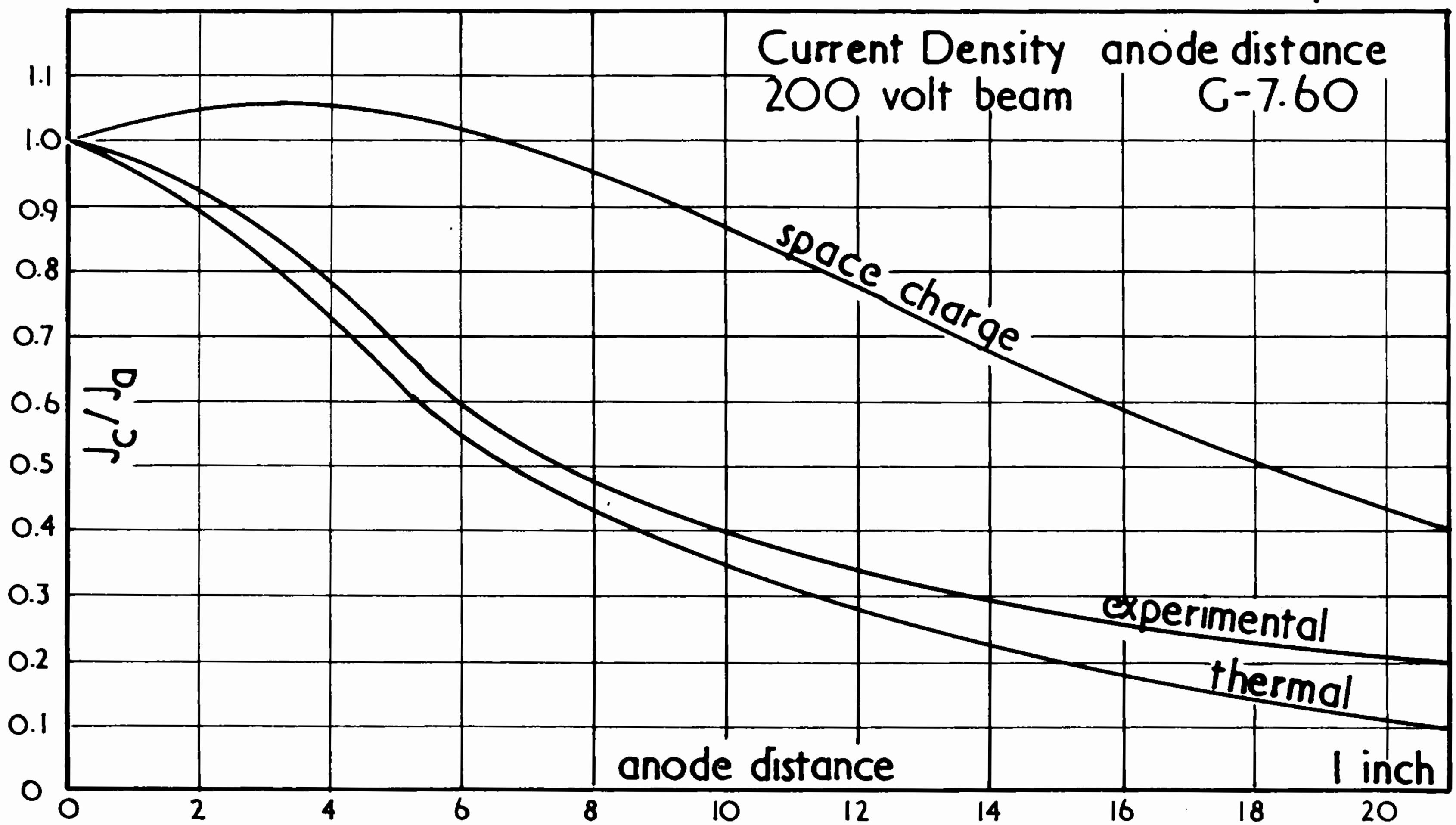
Current Density anode distance
200 volt beam G-7.60
space charge
experimental
thermal
anode distance
1 inch
$J_c/J_a$
1.1
1.0
0.9
0.8
0.7
0.6
0.5
0.4
0.3
0.2
0.1
0
0
2
4
6
8
10
12
14
16
18
20

Graph 9

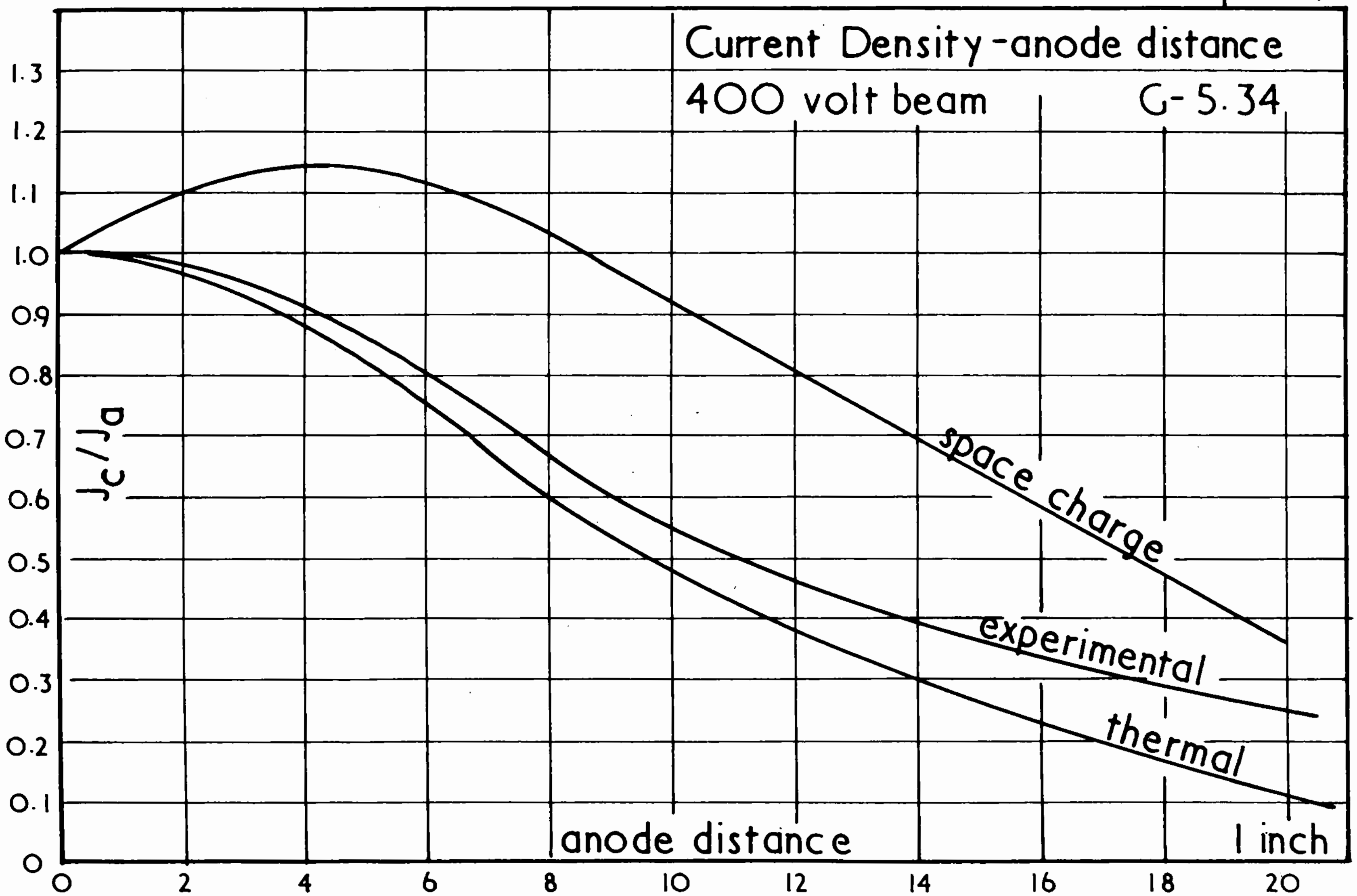
Current Density -anode distance
400 volt beam
G- 5.34
1.3
1.2
1.1
1.0
0.9
0.8
0.7
0.6
0.5
0.4
0.3
0.2
0.1
0
$J_c/J_a$
space charge
experimental
thermal
anode distance
1 inch
0
2
4
6
8
10
12
14
16
18
20

Graph 10

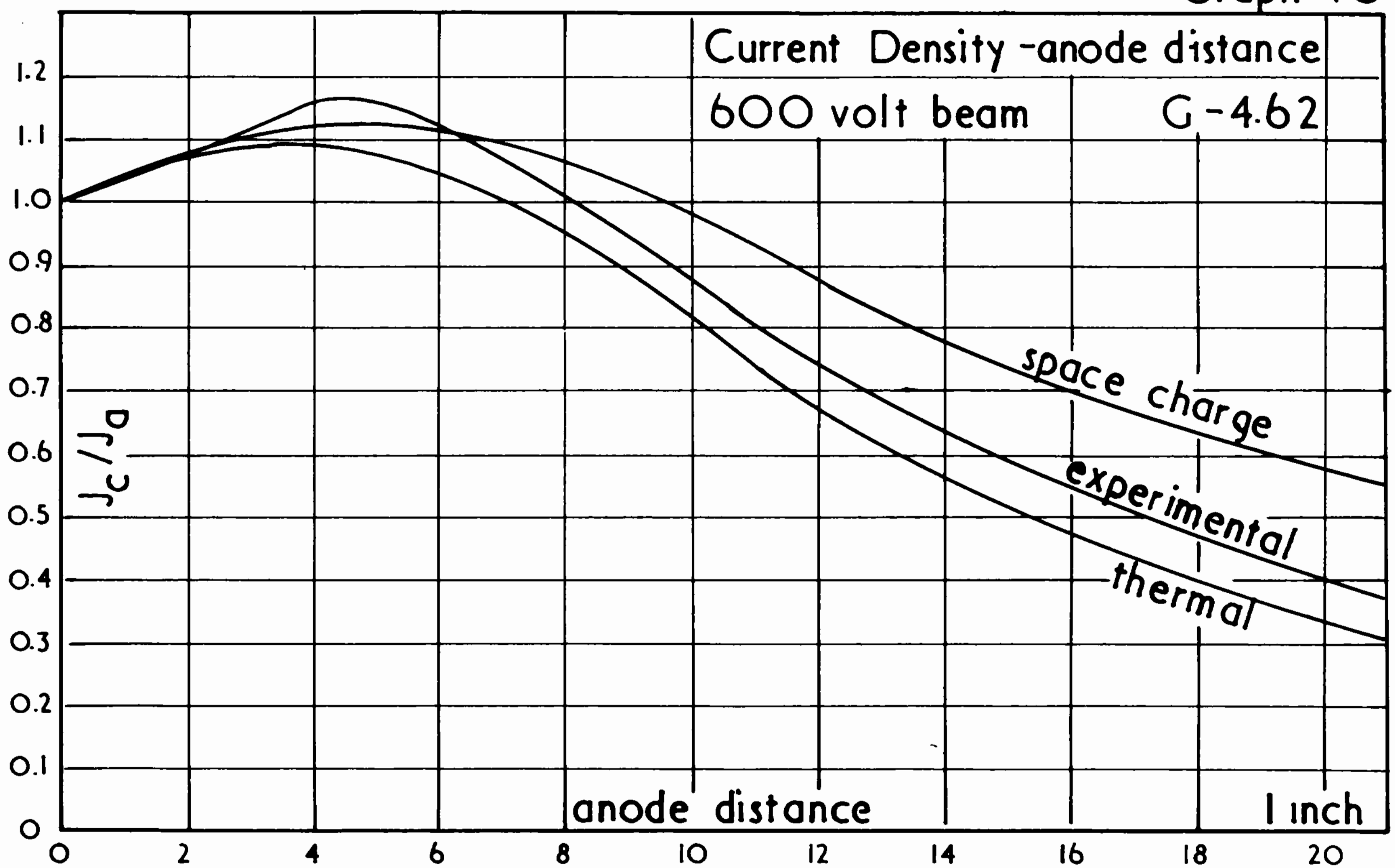
Current Density -anode distance
600 volt beam
G-4.62
$J_c/J_a$
1.2
1.1
1.0
0.9
0.8
0.7
0.6
0.5
0.4
0.3
0.2
0.1
0
0
2
4
6
8
10
12
14
16
18
20
anode distance
1 inch
space charge
experimental
thermal

Graph 11

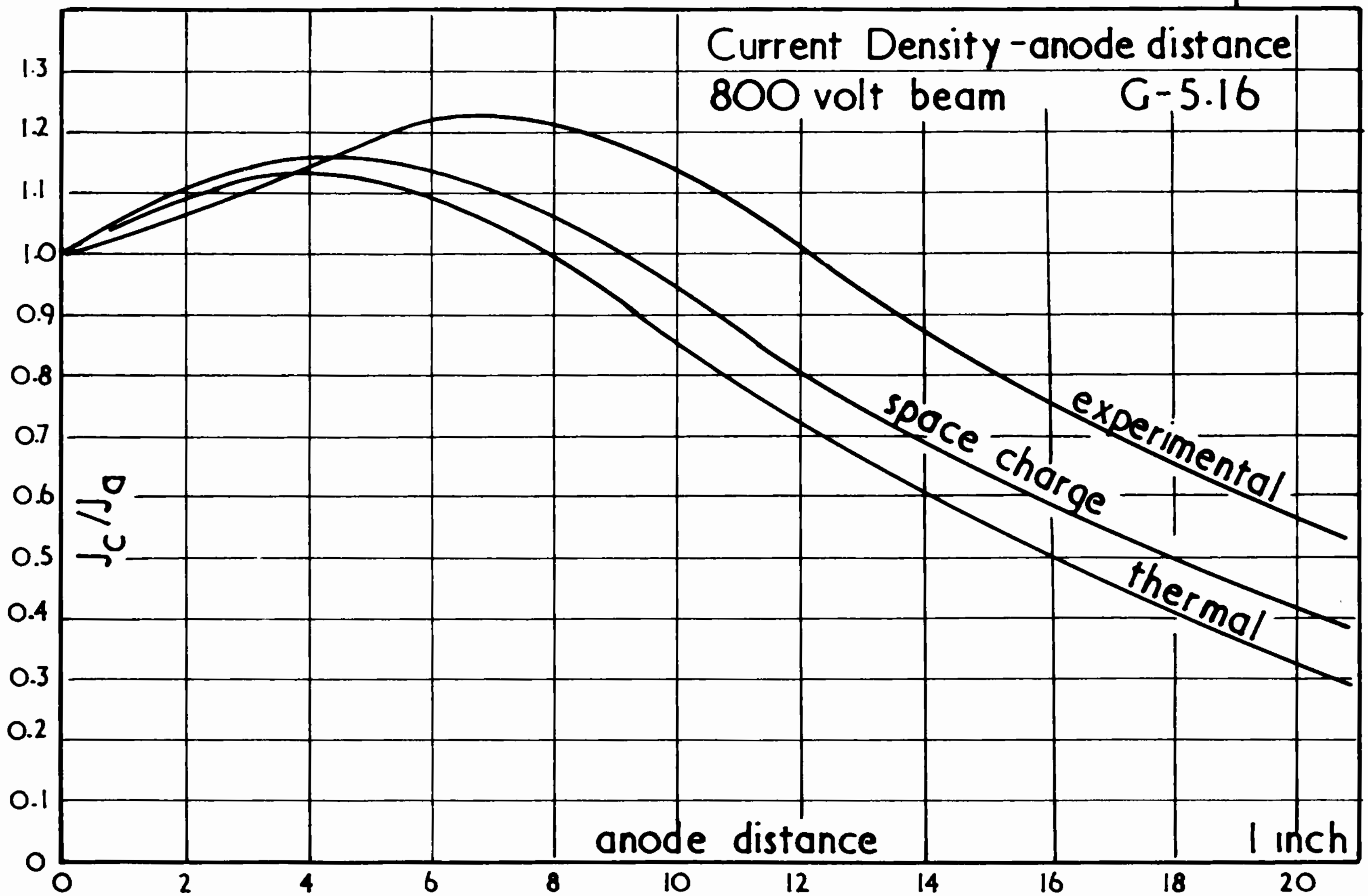

Current Density-anode distance
800 volt beam
G-5.16
$J_c/J_a$
1.3
1.2
1.1
1.0
0.9
0.8
0.7
0.6
0.5
0.4
0.3
0.2
0.1
0
experimental
space charge
thermal
anode distance
1 inch
0
2
4
6
8
10
12
14
16
18
20

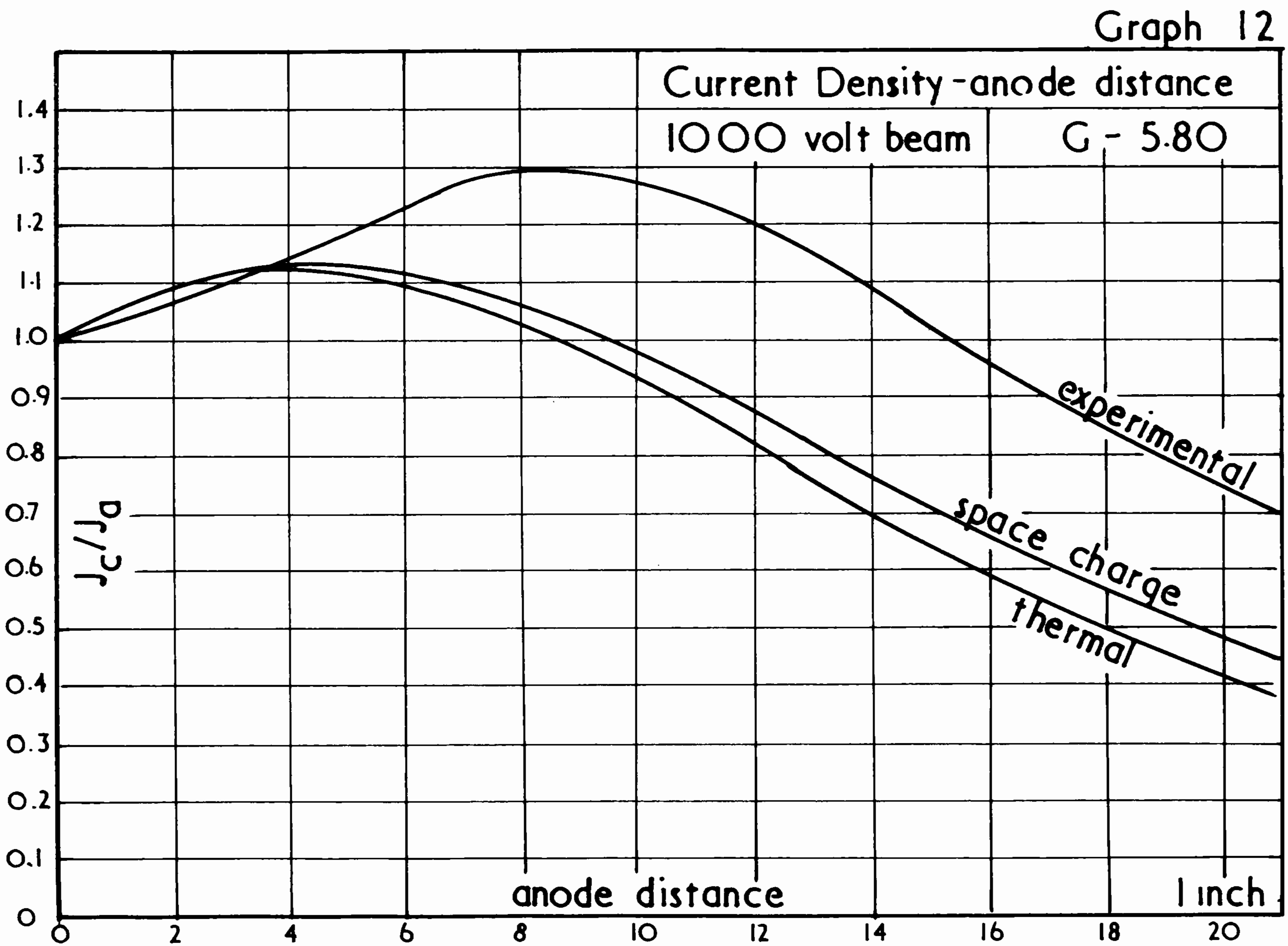
Graph 12
Current Density-anode distance
1000 volt beam
G - 5.80
$J_c/J_a$
1.4
1.3
1.2
1.1
1.0
0.9
0.8
0.7
0.6
0.5
0.4
0.3
0.2
0.1
0
0
2
4
6
8
10
12
14
16
18
20
anode distance
1 inch
experimental
space charge
thermal

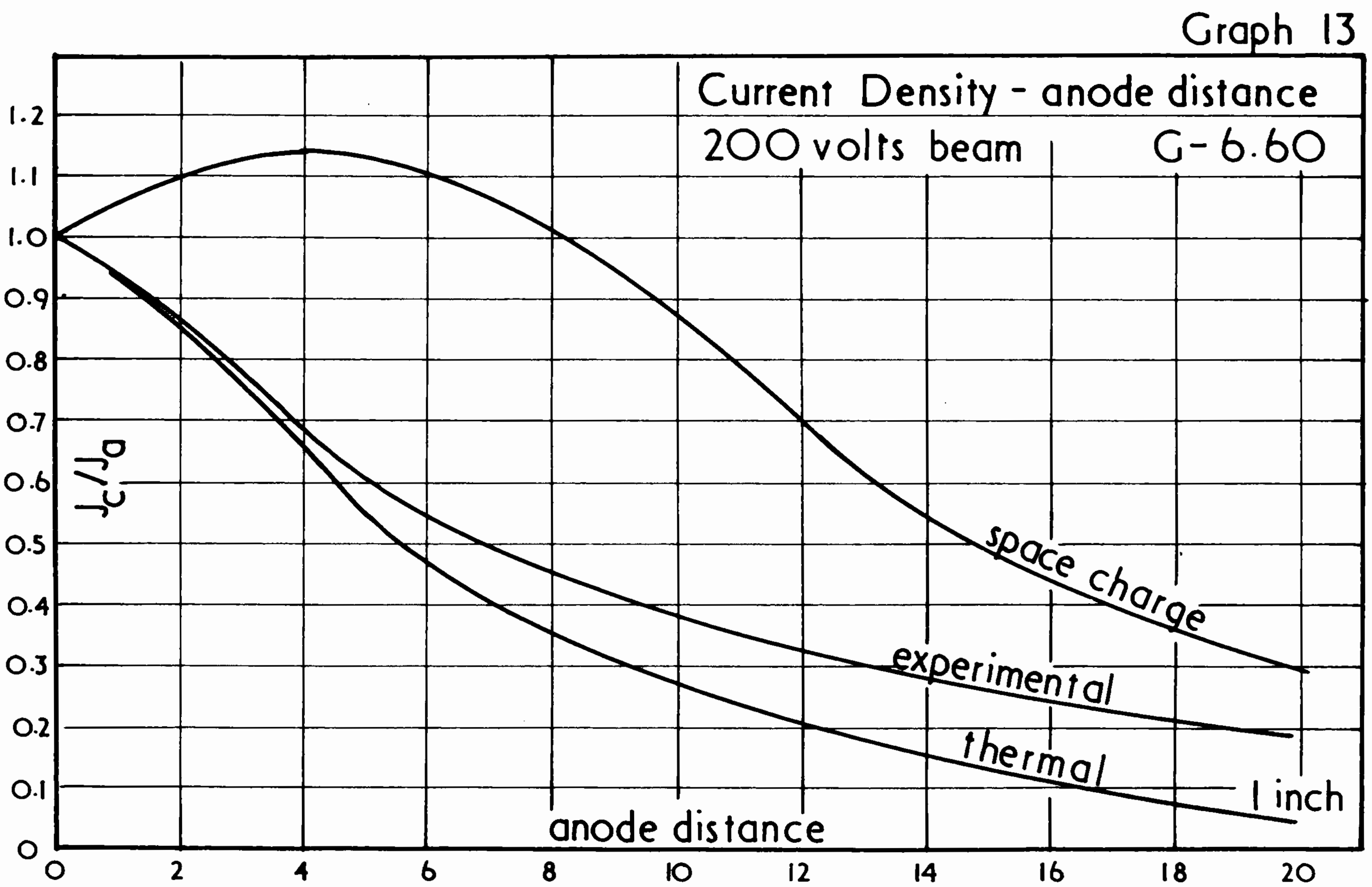

Graph 13
Current Density - anode distance
200 volts beam
G-6.60
$J_c/J_a$
1.2
1.1
1.0
0.9
0.8
0.7
0.6
0.5
0.4
0.3
0.2
0.1
0
space charge
experimental
thermal
1 inch
anode distance
0
2
4
6
8
10
12
14
16
18
20

Graph 14

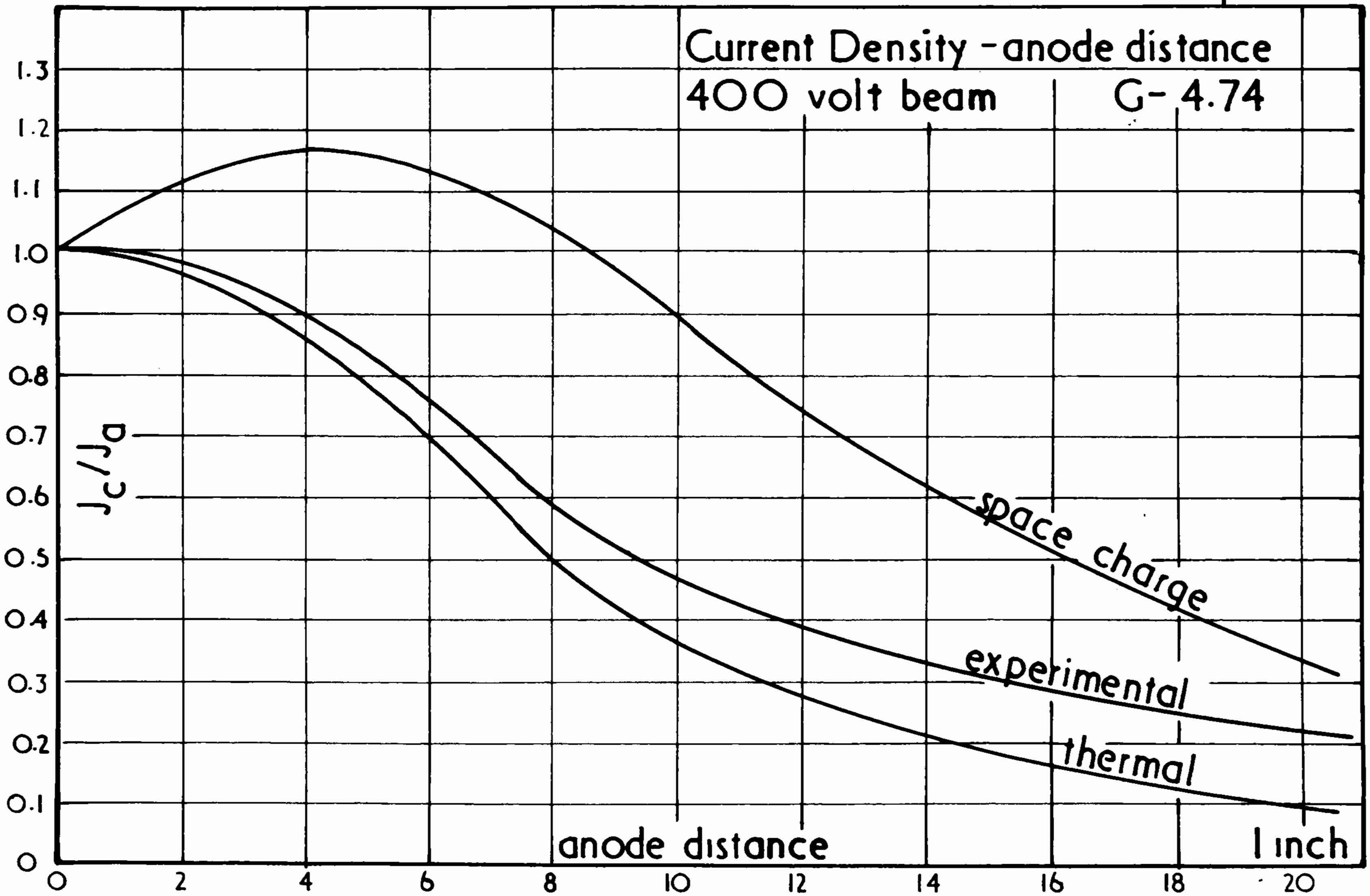
Current Density - anode distance
400 volt beam
G- 4.74
$J_c/J_a$
1.3
1.2
1.1
1.0
0.9
0.8
0.7
0.6
0.5
0.4
0.3
0.2
0.1
0
0
2
4
6
8
10
12
14
16
18
20
anode distance
1 inch
space charge
experimental
thermal

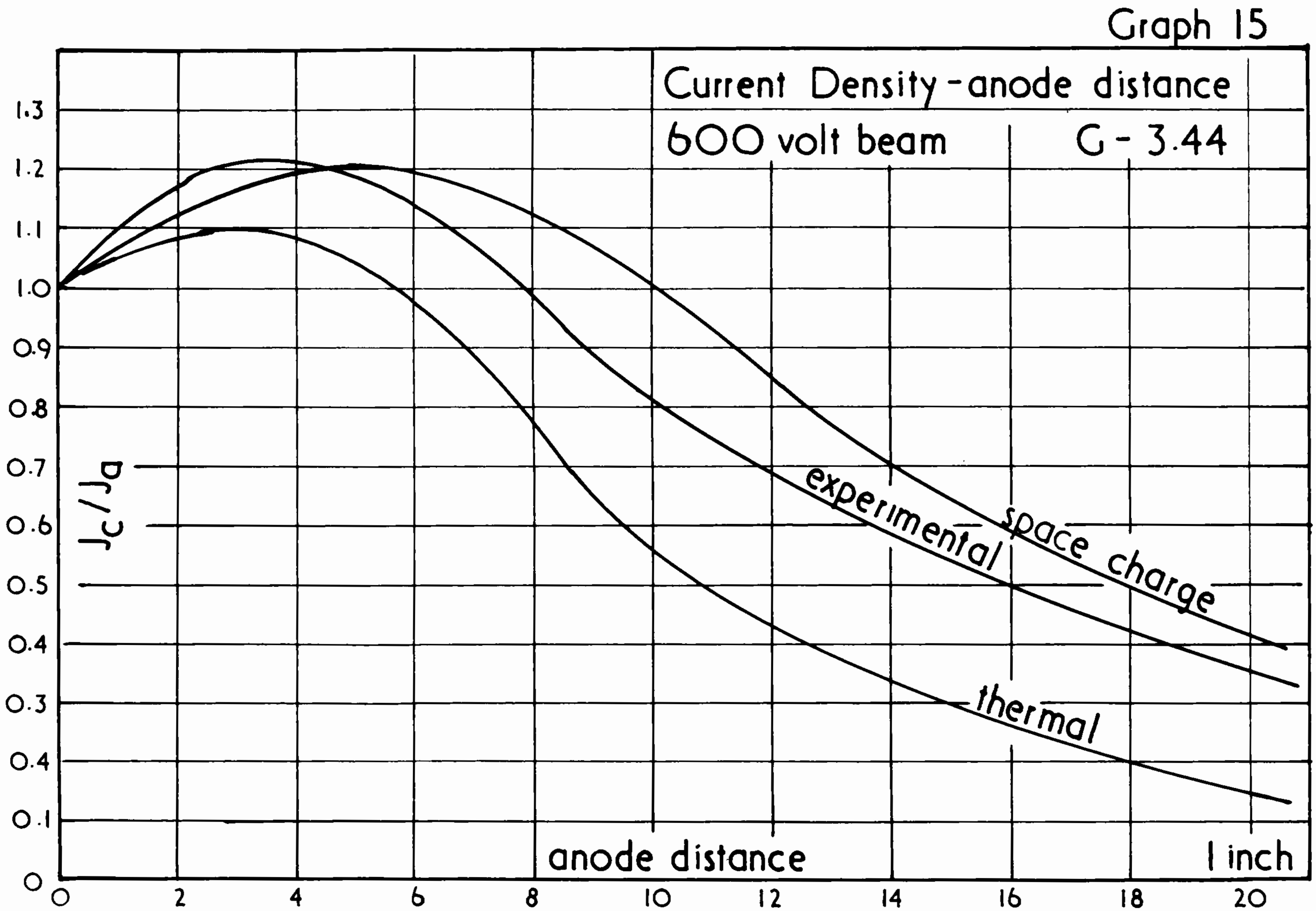

Graph 15
Current Density-anode distance
600 volt beam
G - 3.44
1.3
1.2
1.1
1.0
0.9
0.8
0.7
0.6
0.5
0.4
0.3
0.4
0.1
0
$J_c/J_a$
experimental
space charge
thermal
anode distance
1 inch
0
2
4
6
8
10
12
14
16
18
20

Graph 16

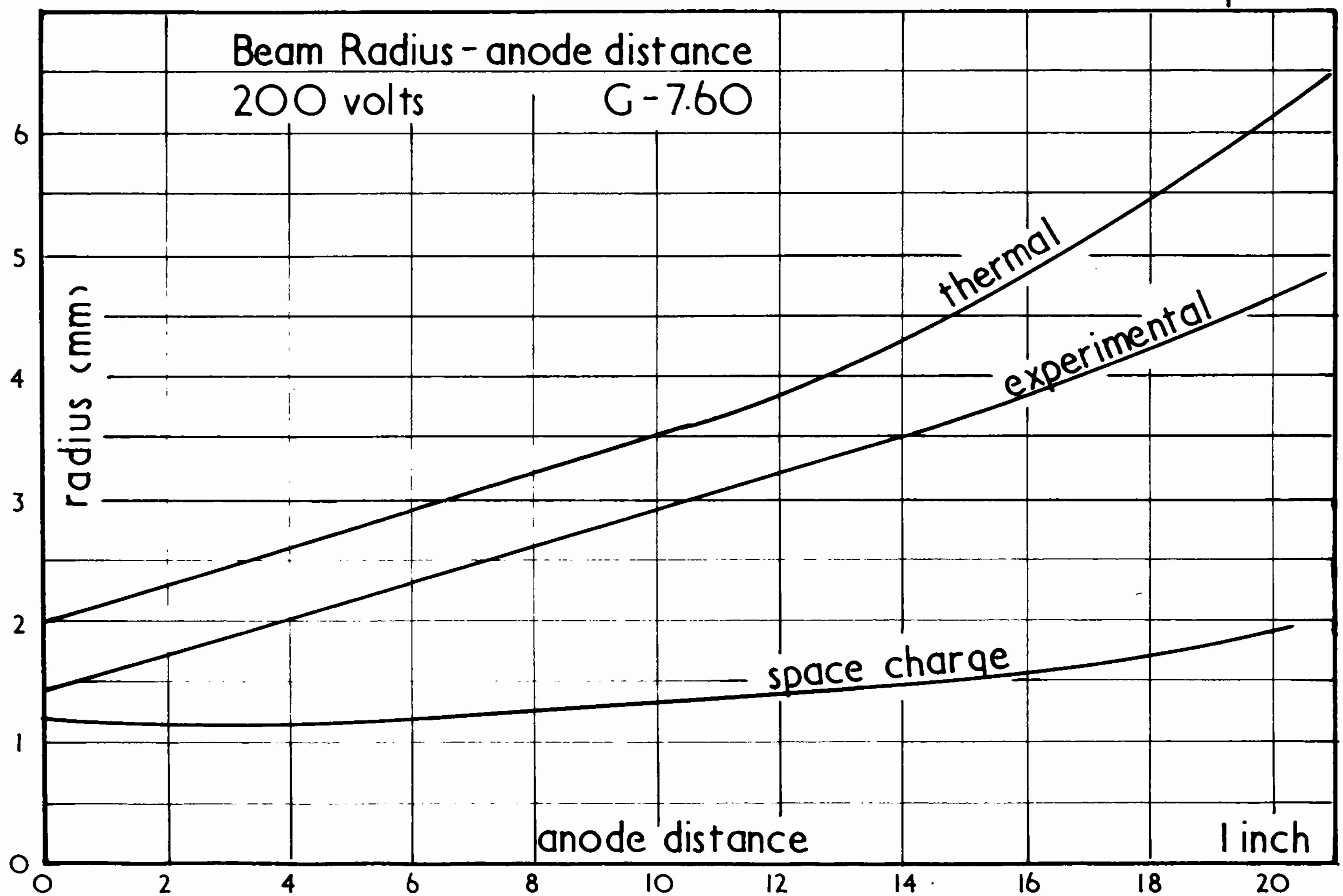

Beam Radius - anode distance
200 volts
G-7.60
radius (mm)
thermal
experimental
space charge
anode distance
1 inch
0
1
2
3
4
5
6
0
2
4
6
8
10
12
14
16
18
20

Graph 17

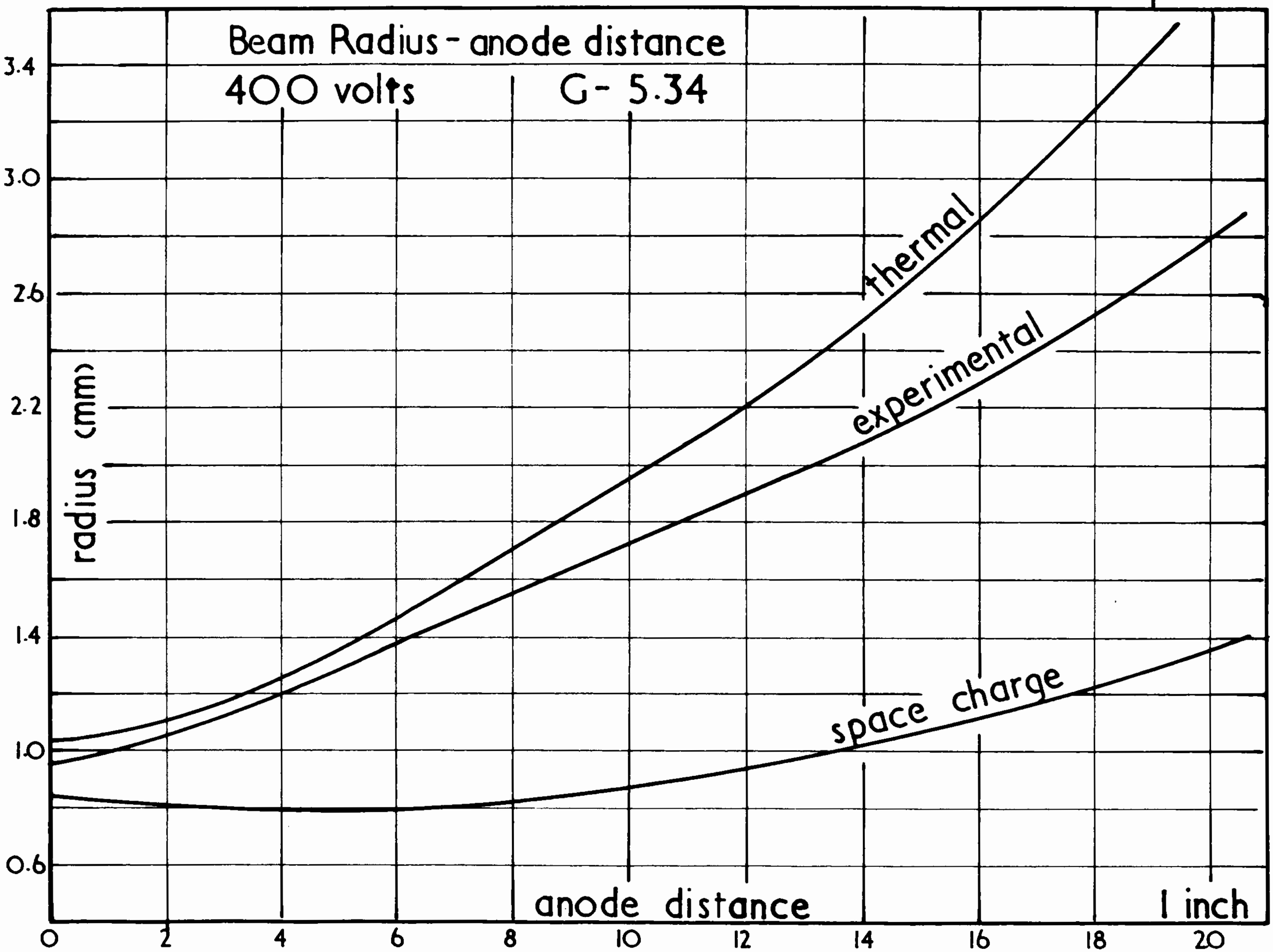
Beam Radius - anode distance
400 volts
G- 5.34
thermal
experimental
space charge
radius (mm)
anode distance
1 inch
3.4
3.0
2.6
2.2
1.8
1.4
1.0
0.6
0
2
4
6
8
10
12
14
16
18
20

Graph 18

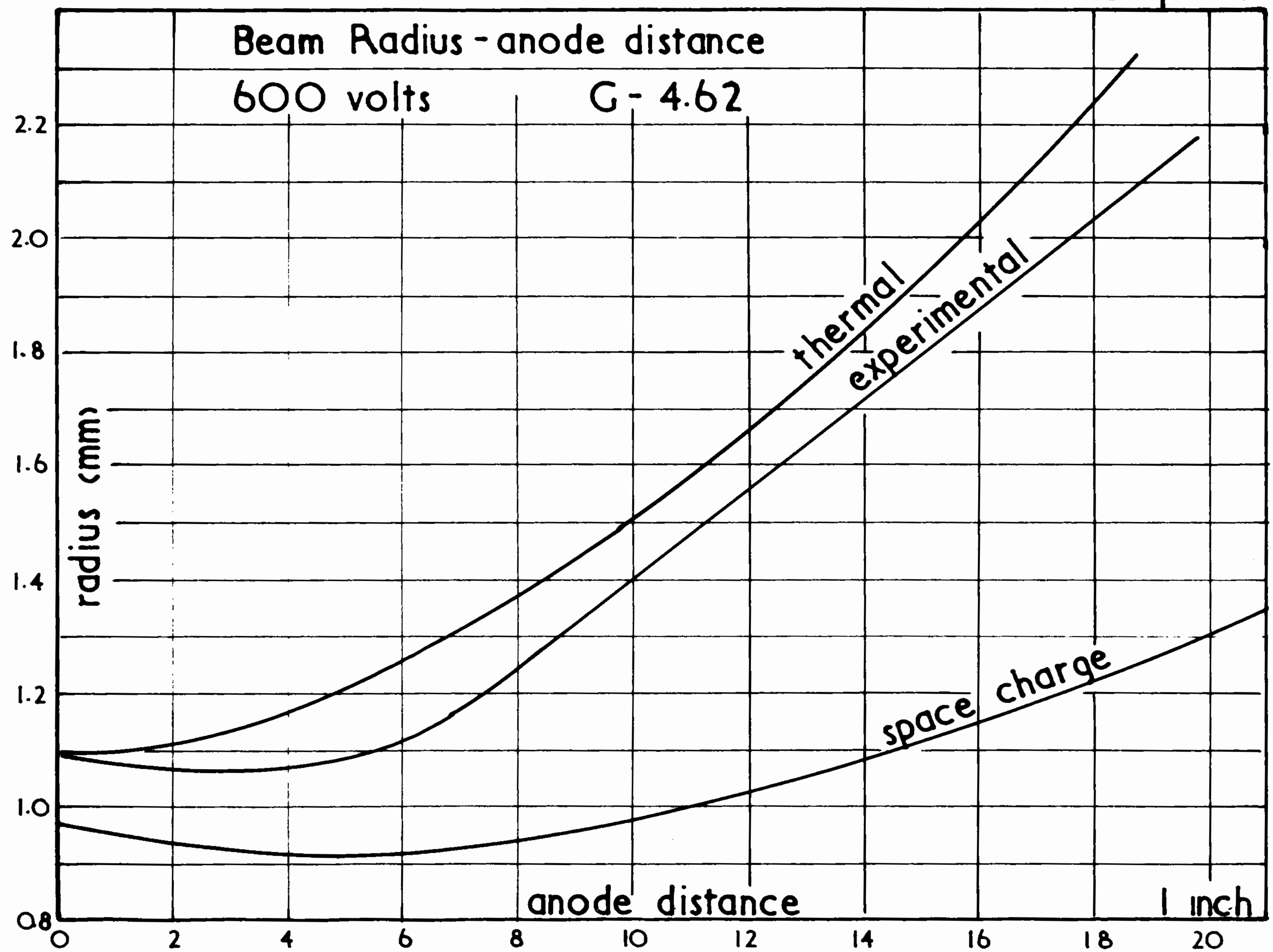
Beam Radius - anode distance
600 volts
G - 4.62
radius (mm)
thermal
experimental
space charge
anode distance
1 inch
2.2
2.0
1.8
1.6
1.4
1.2
1.0
0.8
0
2
4
6
8
10
12
14
16
18
20

Graph 19

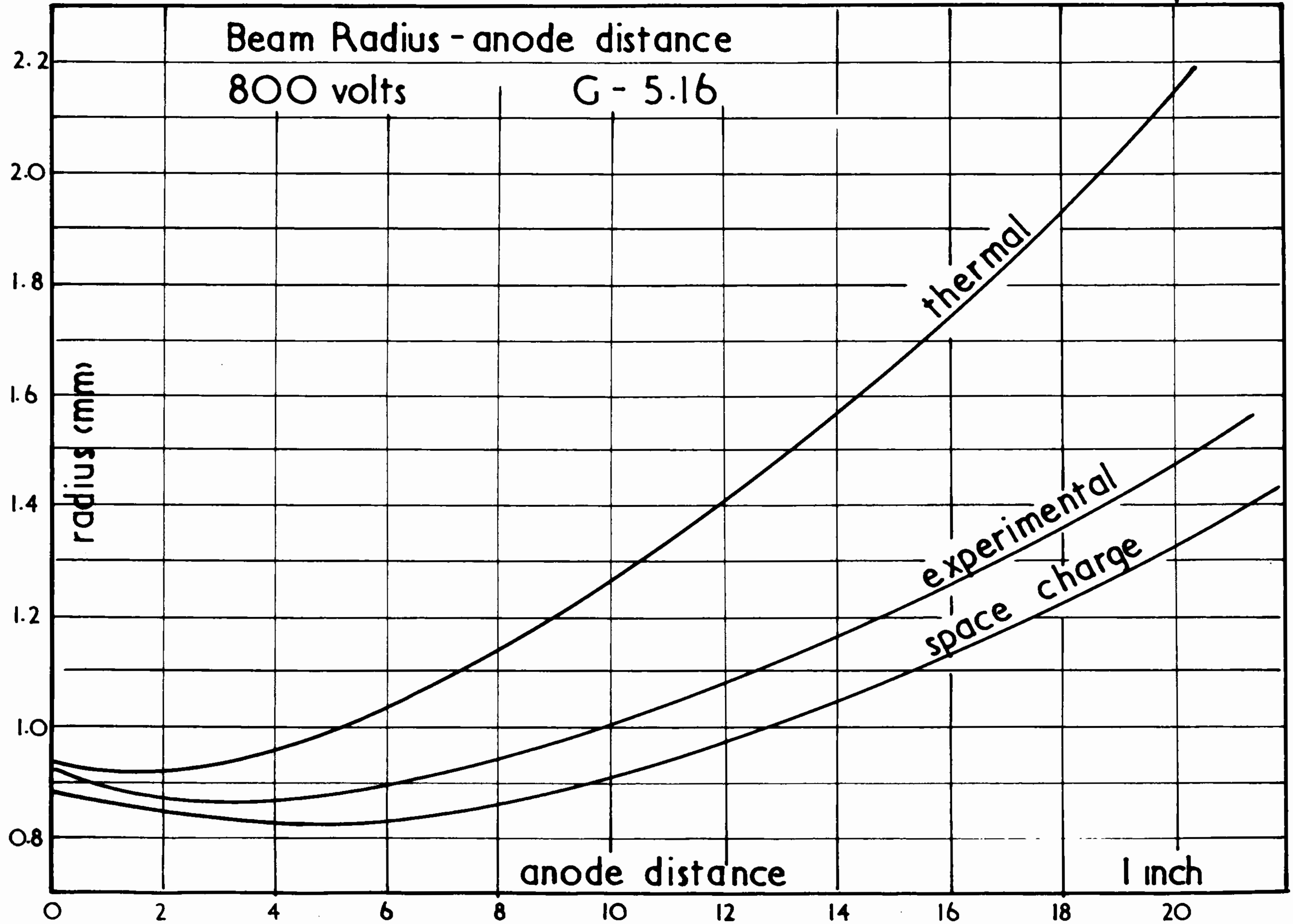
Beam Radius - anode distance
800 volts
G - 5.16
thermal
experimental
space charge
radius (mm)
anode distance
1 inch
2.2
2.0
1.8
1.6
1.4
1.2
1.0
0.8
0
2
4
6
8
10
12
14
16
18
20

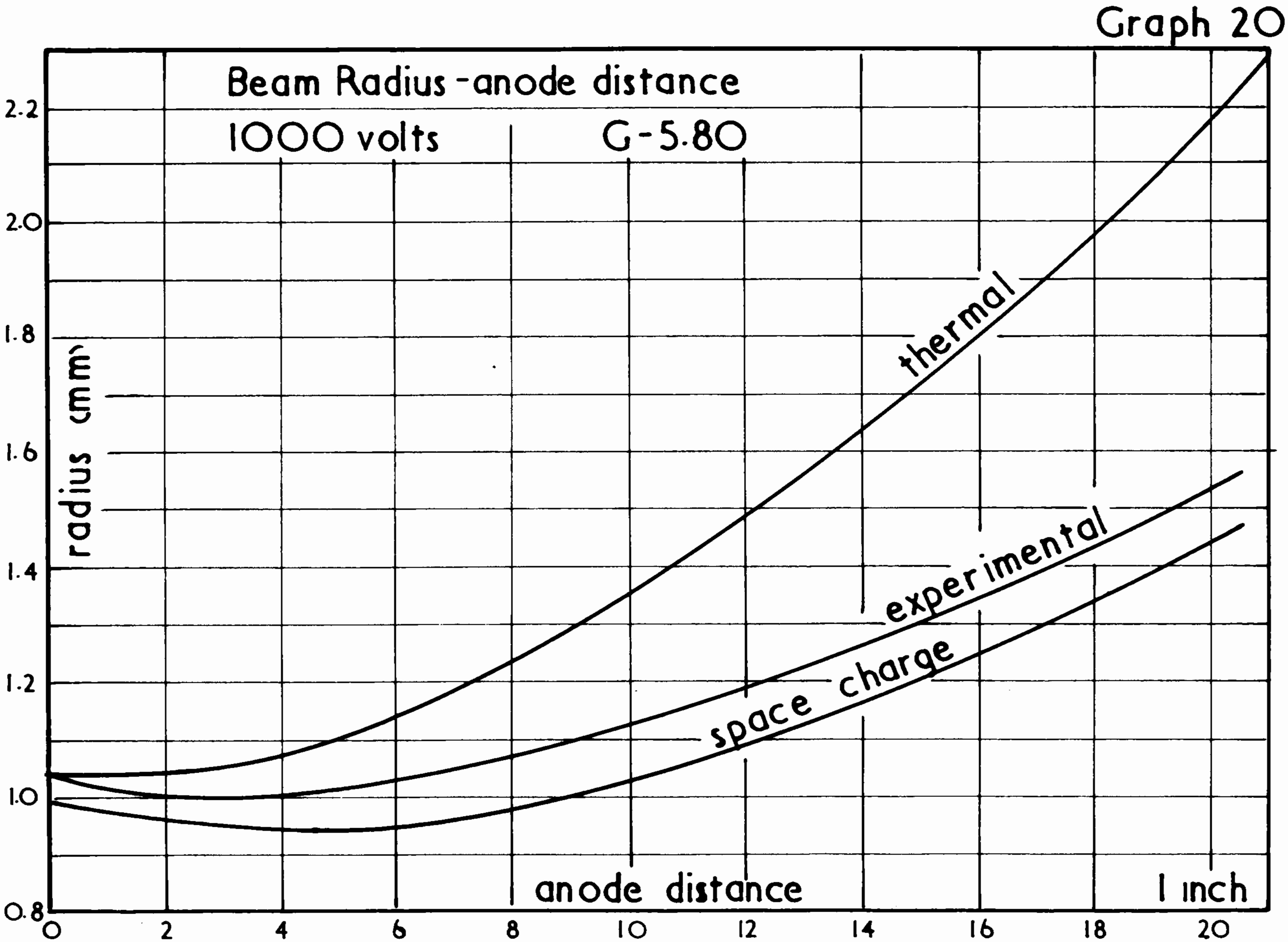
Graph 20
Beam Radius - anode distance
1000 volts
G - 5.80
radius (mm)
thermal
experimental
space charge
anode distance
1 inch
2.2
2.0
1.8
1.6
1.4
1.2
1.0
0.8
0
2
4
6
8
10
12
14
16
18
20

Graph 21

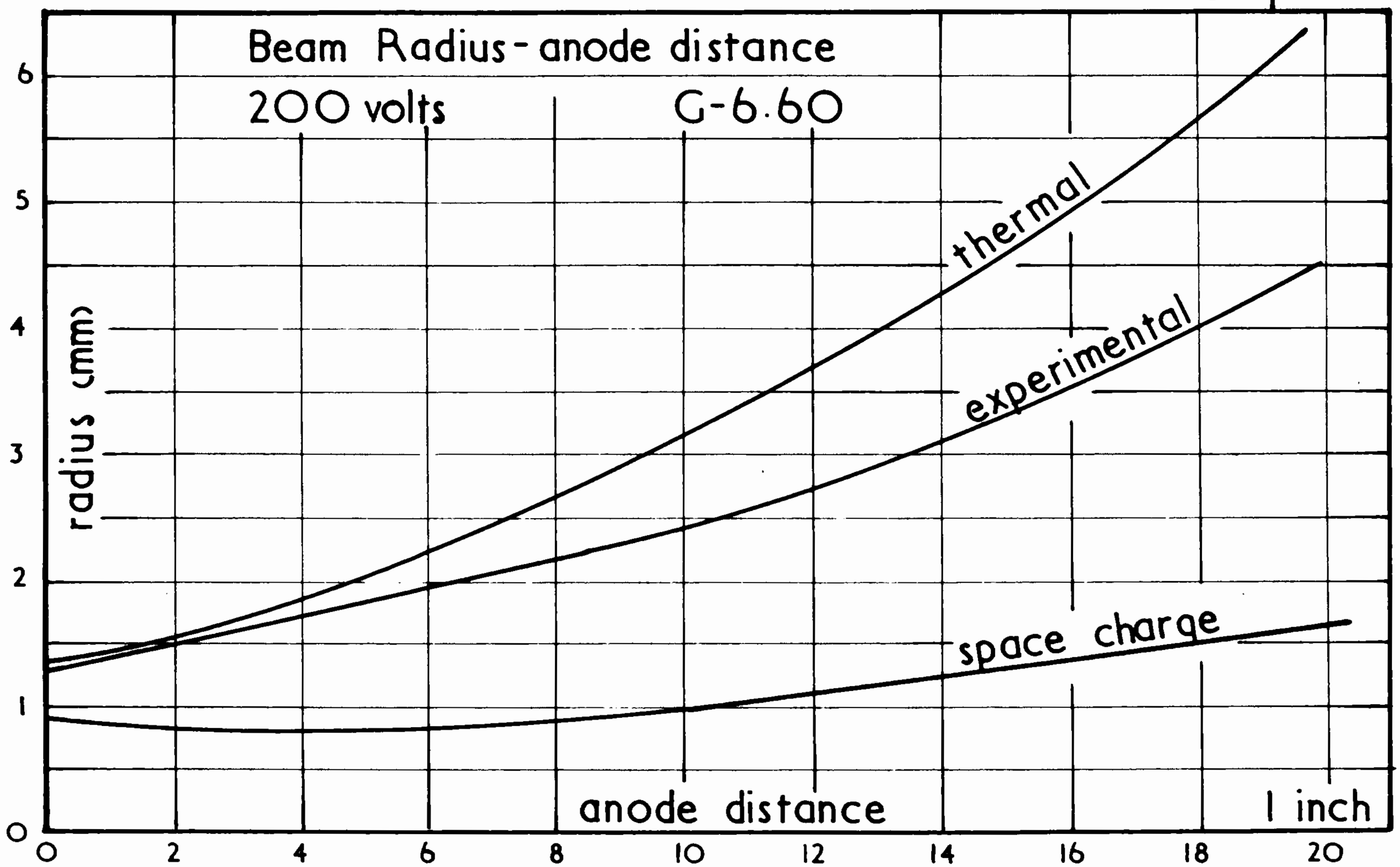

Beam Radius - anode distance
200 volts
G-6.60
thermal
experimental
space charge
radius (mm)
anode distance
1 inch
0
1
2
3
4
5
6
0
2
4
6
8
10
12
14
16
18
20

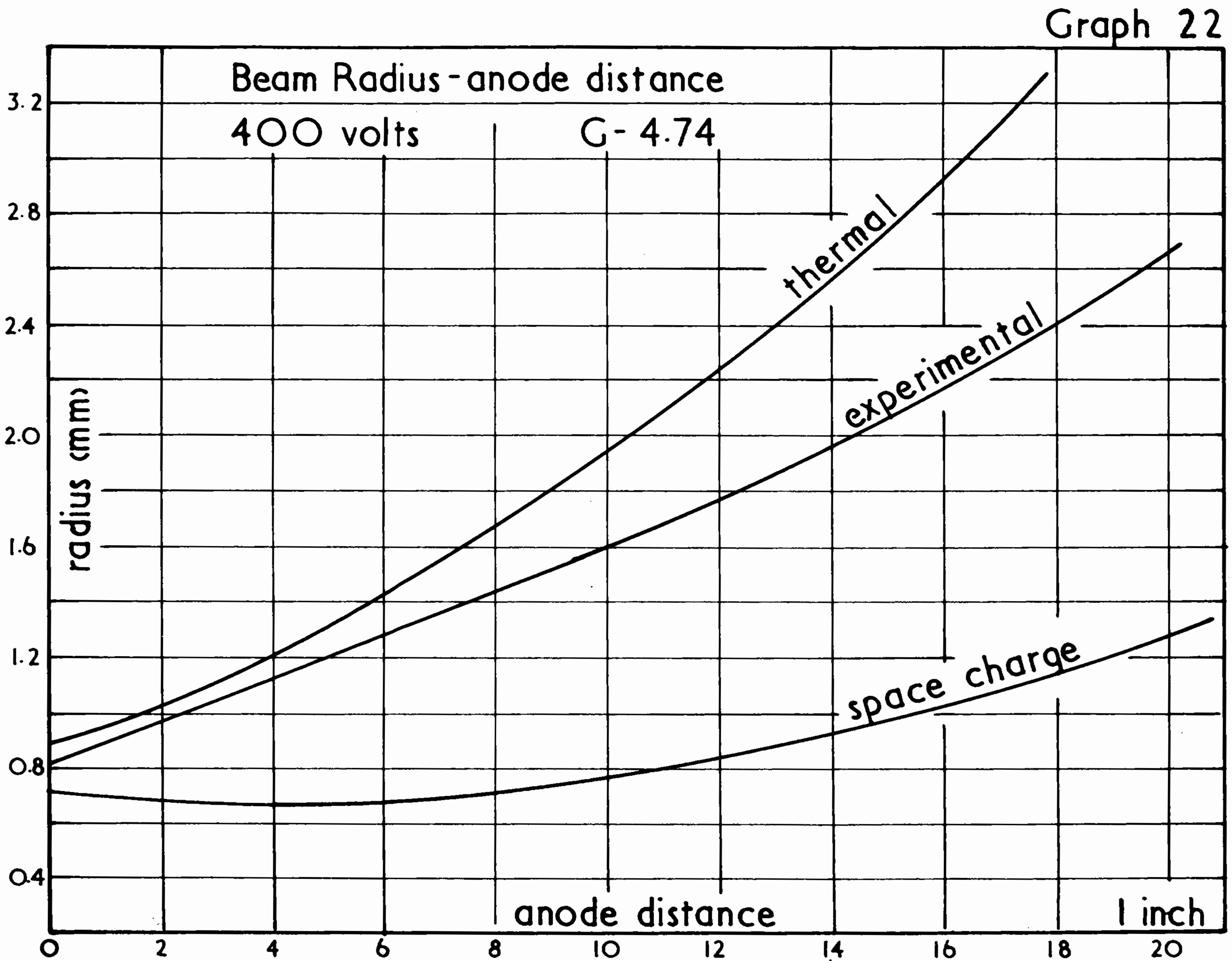
Graph 22
Beam Radius - anode distance
400 volts
G - 4.74
thermal
experimental
space charge
radius (mm)
anode distance
1 inch
3.2
2.8
2.4
2.0
1.6
1.2
0.8
0.4
0
2
4
6
8
10
12
14
16
18
20

Graph 23

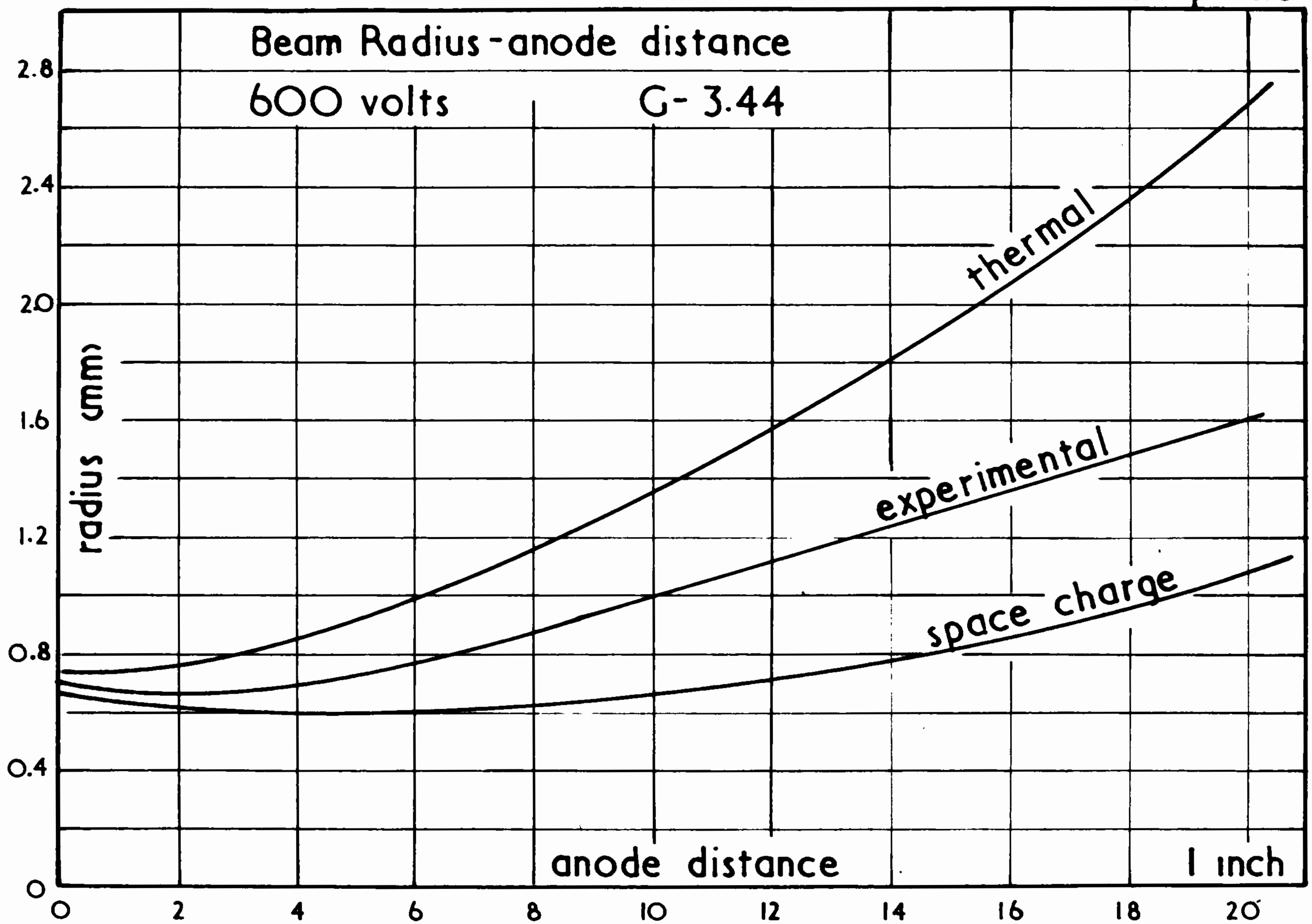
Beam Radius - anode distance
600 volts
G- 3.44
thermal
experimental
space charge
radius (mm)
anode distance
1 inch
2.8
2.4
2.0
1.6
1.2
0.8
0.4
0
0
2
4
6
8
10
12
14
16
18
20

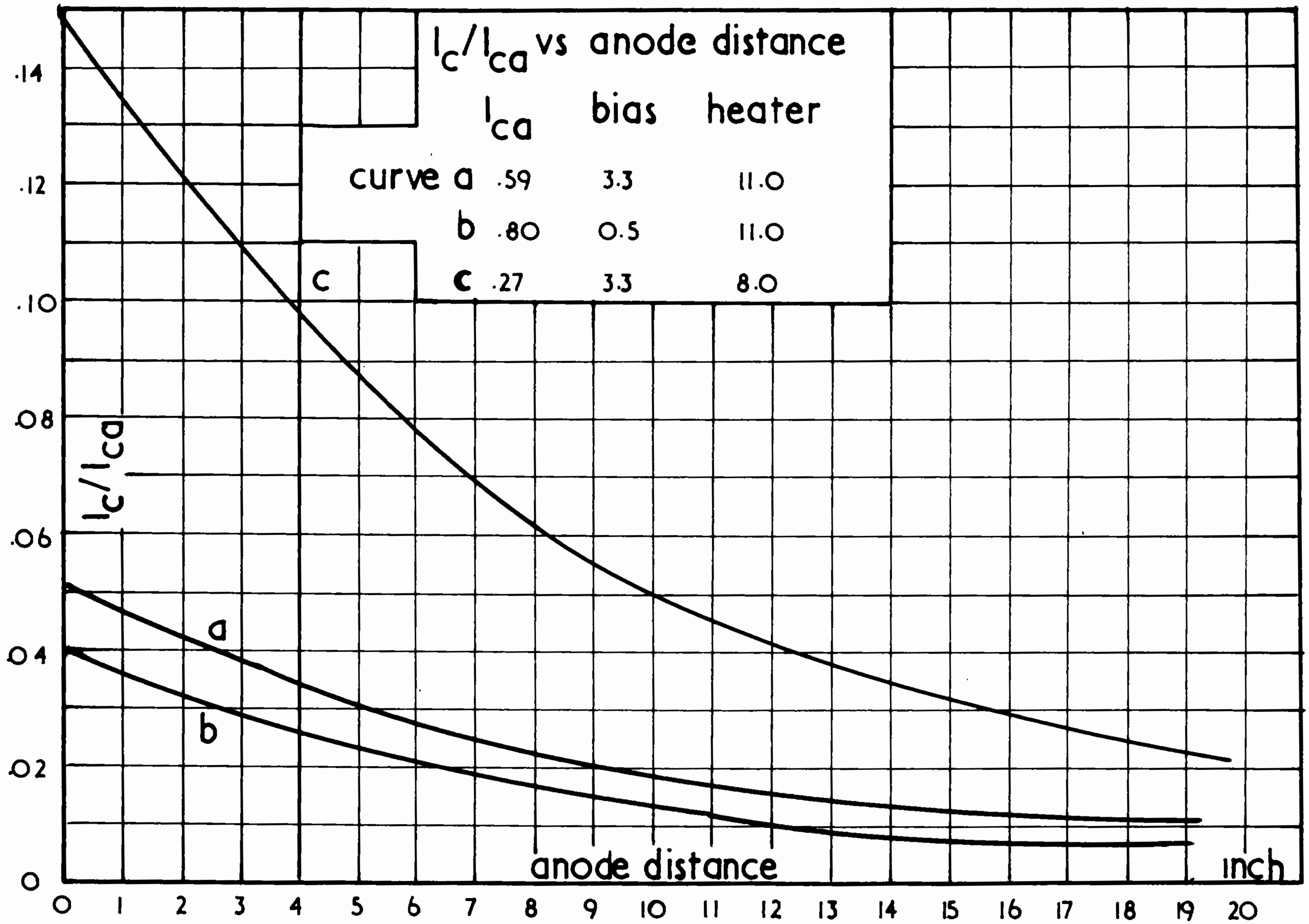


Beam Voltage - 200

Graph 24

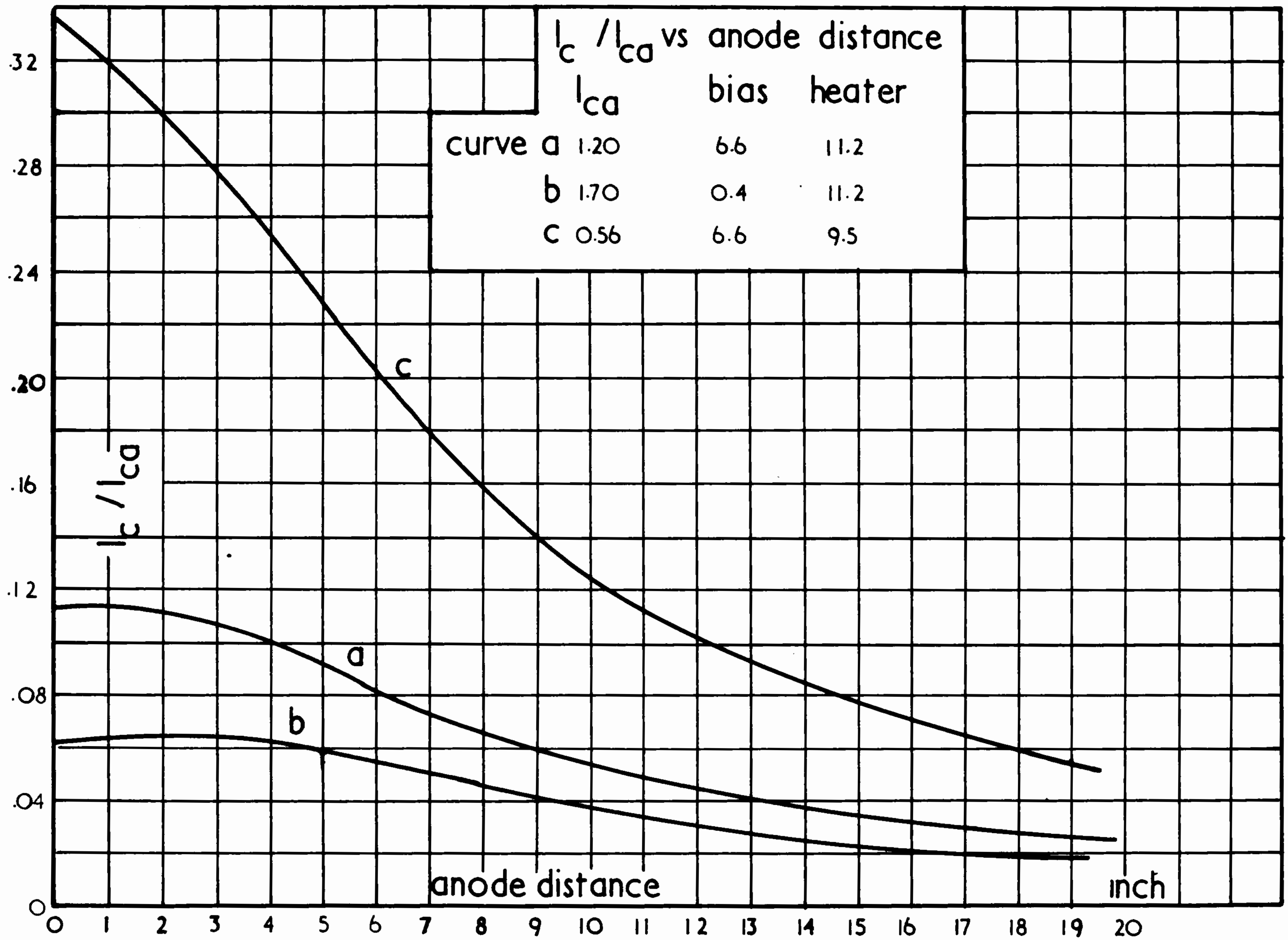


Beam Voltage - 400

Graph 25

# 4. CONCLUSIONS.

## 4.1. Oxide Cathodes.

Oxide cathodes made with the materials and in the manner described can give satisfactory continuous performance at pressures up to $8 \times 10^{-7}$ mm.Hg. with an anode voltage below 800 volts. Continuous emission above 1000 volts requires a pressure better than $2 \times 10^{-7}$ mm.Hg. Even after severe poisoning, the cathodes may be reactivated from three to four times, but after the initial activation, forepump pressure, at least, must be maintained in the vacuum system at all times. In the system used, the cathode was effectively isolated from the active oil diffusion pump, by a liquid-air cold trap.

## 4.2. Pierce Guns.

The Pierce gun, with simplified straight line electrode shapes was satisfactory in all aspects of its performance. Its manufacture was convenient and accurate and its self-alignment must be considered excellent. The partition was essentially 100% over the range 100 to 1700 volts, and the perveance constant but 8% higher than predicted by theory.

The cathode electrode bias can be used as a "grid" - to control the current emitted from the gun - although this results in a "defocus" of the beam. Under proper working conditions beam current densities of 200 milliamperes per square centimeter can be obtained at the beam minimum.

The consideration of the effect of the anode aperture, based on the plotting of the electric fields present, yielded a satisfactory prediction of the beam behaviour on leaving the gun.

4.3. Beam Spreading.

At pressures below $5 \times 10^{-7}$, the beam spreading measured agreed closely with that predicted by the theory of Cutler and Hines. In all cases the spreading was less than theoretically expected although to what extent this is due to positive ion neutralisation is difficult to estimate.

At pressures near $10^{-6}$ mm., the effect of positive ions was such as to reduce space charge spreading considerably, although it seems the space charge prediction could be used to give a minimum beam radius. The beam minima are definitely shifted from the space charge position by thermal velocities towards the anode. This was observed at all pressures even though the effect of positive ions would be to "push" the minima further from the anode. This phenomenon of the shift in the position of the beam minimum is an important one. If it is desired, as is often the case in travelling wave tubes, to obtain magnetically focussed Brillouin flow in the beam, the position of its minimum must be known, for it is imperative that the magnetic fields "start" here at the position where the electrons have no radial velocity.

The effect of thermal velocities was shown in a different way in Graphs 24 and 25. In view of the information shown in these graphs, it may well be that the greatly improved gun performance in the present work owes much to the use of an oxide cathode emitter. The emitters of previous guns, as mentioned earlier, were tungsten filaments. These are operated at temperatures close to 2000$^{\circ}$K, as contrasted to the oxide cathode's running temperature of 1100$^{\circ}$K. There would be considerably more thermal velocity spreading with the former, which could easily account for the poor gun partition obtained.

## LIST OF REFERENCES.


(1) "Theory and Design of Electron Beams" - J.R. Pierce. D. Van Nostrand Co. 1949.

(2) "Electron Guns" - R.F.C. Vessot. M.Sc. Thesis, McGill University. 1954.

(3) "Thermal Velocity Effects in Electron Guns" - Cutler and Hines. Proc.I.R.E. March 1955.

(4) M.I.T. Tube Laboratory Manual.

(5) E.H. Blevis - M.Sc. Thesis. McGill University. 1956.

(6) A. Szabo - M.Sc. Thesis. McGill University. 1955.

(7) "Pin Hole Camera Investigation of Electron Beams" - Cutler and Saloom. Proc.I.R.E. March 1955.

## BIBLIOGRAPHY.


"Theory and Design of Electron Beams" - J.R. Pierce, D.Van Nostrand Co. 1949.

"Thermal Velocity Effects in Electron Beams" - Cutler and Hines. Proc.I.R.E. March 1955.

"Pin Hole Camera Investigation of Electron Beams" - Cutler and Saloom. Proc.I.R.E. March 1955.

"Vacuum Tubes" - K. Spangenberg - McGraw Hill. 1948.

"Electron Guns" - R.F.C. Vessot - M.Sc. Thesis - McGill University.

"Notes on Design of Electron Guns" - A.L. Samuel. Proc.I.R.E. April 1945.

"High Current Electron Guns" - L.M. Field. Rev.Mod.Phys.July 1946. vol.18.

"Effect of Anode Aperture on Potential Distribution" - Brown and Susskind. Letter to I.R.E. March 1954.

"The Oxide Coated Cathode" - Hermann and Wagner. Chapman and Hall, 1951.

"Formation and Maintenance of Electron Beams" - Smith and Hartman. Journal App.Phys. March 1940. vol.11.

"Space Charge Limitations on the Focus of Electron Beams" - Thompson and Headrick. Proc.I.R.E. July 1940.

"Brillouin Flow and Thermal Velocities" - Pierce and Walker. Journal App.Phys. October 1953.